공학석사 학위논문

Synthesis of nano $ZnGa_2O_4$ Spinel Phosphor via Novel Liquid-Phase Combustion Method

Novel 용액연소법을 이용한 나노 $ZnGa_2O_4$

스피넬 형광체 합성법

2013년 8월

서울대학교 대학원

재료공학부

이 문 균

Synthesis of nano $ZnGa_2O_4$ Spinel Phosphor via Novel Liquid-Phase Combustion Method

A DISSERTATION SUBMITTED TO
DEPARTMENT OF MATERIALS SCIENCE AND ENGINEERING
SEOUL NATIONAL UNIVERSITY

FOR THE DEGREE OF
MASTER OF SCIENCE

Mun Keun Lee

August 2013

Synthesis of nano $ZnGa_2O_4$ Spinel Phosphor via Novel Liquid-Phase Combustion Method

지도교수 강 신 후

이 논문을 공학석사 학위논문으로 제출함

2013년 8월

서울대학교 대학원

재료공학부

이 문 균

이문균의 석사학위논문을 인준함

2013년 8월

위 원 장 남 기 태 (인)

부위원장 강 신 후 (인)

위 장 홍 성 현 (인)

Abstract

Wide band gap oxide semiconductors such as zinc gallate ($ZnGa_2O_4$) is gaining great attention in recent years due to its great potential as a phosphor host material with prospective applications as UV (ultraviolet) emitter in diverse field of areas including field emission display (FED), thin-film electroluminescent displays. $ZnGa_2O_4$ as an oxide-based spinel structured phosphors has better physical and chemical properties than conventional sulphide phosphors, along with interesting optical properties making it an interesting material to study. Moreover, the introduction of nanosized product will enable even wider range of functions in other fields of nano-science and technology.

Although many synthesizing methods have been proposed, in this dissertation, liquid-phase semi-combustion method developed by our laboratory was used to synthesize $ZnGa_2O_4$ nanosized particles through stoichiometrically balanced system between metal-organic precursors and organic fuel, urea, for a complete redox reaction to obtain about 5 nm in particle size. The optical properties of $ZnGa_2O_4$ were studied along with investigation and characterization of undoped and doped with transition metals (chromium and titanium) for tuneable emission in photoluminescence (PL) properties obtaining blue, red and bluish white colours. The intrinsic blue PL emission originated from a transition via a self-activation centre between Ga-O under excitation 280 nm in wavelength. These emission characteristics were further confirmed using photoluminescence spectra and explained using the energy diagrams.

The band gap energy (Eg) of $ZnGa_2O_4$ was calculated as 5 eV using the first-principle approach, Discrete Variational Xα (DV-Xα), which converges

congruently with literature values, but for more precise calculation further work on oxygen vacancy will be required. Moreover, strong red and bluish white emissions were observed by doping it with transition metals: $ZnGa_2O_4$:Cr^{3+} and $ZnGa_2O_4$:Ti^{3+} respectively, without the use of rare-earth materials and therefore diminishing the material cost.

Furthermore, a non-stoichiometrically balanced redox system was used to investigate the physical effect of organic impurities on $ZnGa_2O_4$ phosphor materials. This non-stoichiometrically balanced redox reaction shows a strong yellow emission and returned to its original blue emission with heat-treatment at 1000℃ for 1 hour, showing very strong stability at high temperature. The possibility of organic bridging or doping of organic impurities were characterised and discussed.

In this dissertation, the understanding of optical properties between bulk and nano-sized undoped and doped-$ZnGa_2O_4$ as well as the effect of organic functional groups were explained with a series of experimental results and discussed in terms of theoretical background.

Key word: $ZnGa_2O_4$, Nanocrystals, Photoluminescence, Organic-Inorganic Hybrid Materials

Student number: 2011-24049

Table of Contents

List of Figures

List of Tables

List of Appendix

Chapter 1. Introduction

1.1. Luminescent Materials

Materials which exhibit luminescent properties are often excited by cathode rays, X-rays, or UV emission of gas discharge, which corresponds to applications in displays, medical imaging and lighting devices. On the short-wavelength end of the visible spectrum is the near-ultraviolet (n-UV) band from 320 to 400 nm, and on the long-wavelength end is the near-infrared (n-IR) band from 750 to approximately 2500 nm. The electromagnetic wavelength and specified colours in the visible range of spectrum can be broken up into the approximate wavelength values as shown in Figure 1 and Table 1.

Luminescent material (phosphor) usually comprises of an inorganic host crystal material and one or more intentionally introduced impurities such as transition metal or rare-earth material, called activators or dopants. These impurity concentrations are generally lowly occupied as higher concentration will decrease its luminescent efficiency[1]. When phosphor materials absorb electromagnetic radiation, it leads to emission of different electromagnetic radiation called the optical excitation. The energy transfer mechanism from host lattice itself (band absorption) to the activator ions (sensitizer) or one dopant (sensitizer) to another (luminescent centre) is sometimes used to enhance the sensitivity of a phosphor, converting certain types of energy into electromagnetic radiation generally in the visible light region. Depending on the source of excitation such as photons, electrons, current, and heat, the phenomena of luminescence can be classified as: photo-, cathode-, electro-, and thermo-luminescence[2].

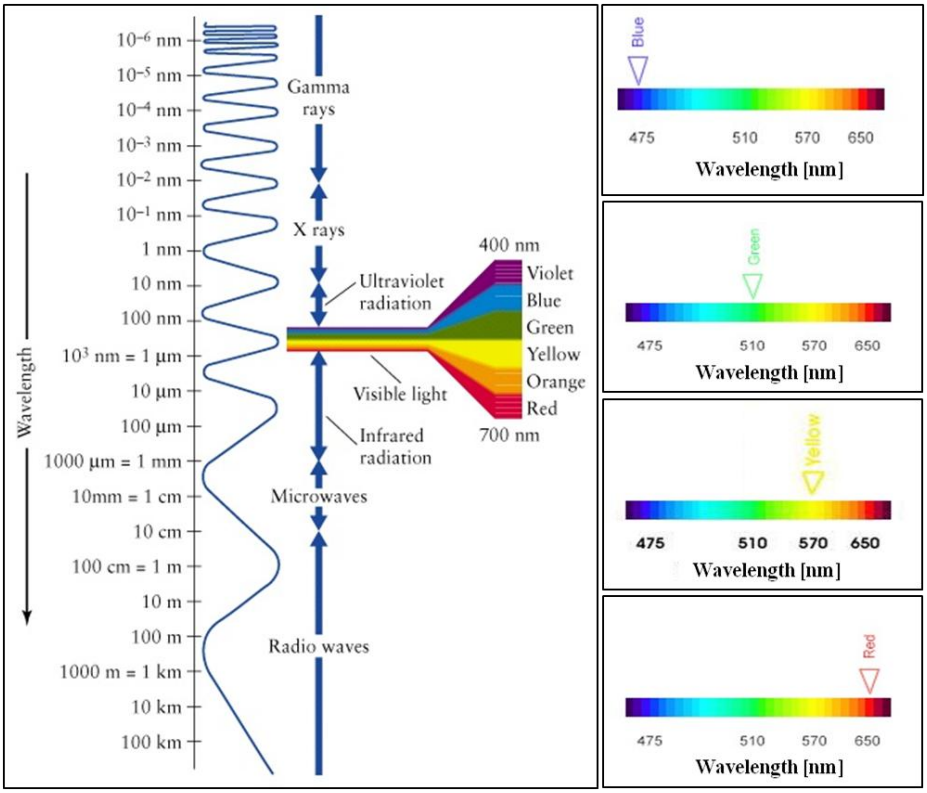

Figure 1. Electromagnetic spectrum labelled "visible light"[3].

Violet and Indigo	**400 – 450nm**
Blue and Aqua	**450 – 500nm**
Green	**500 – 570nm**
Yellow and Orange	**570 – 610nm**
Red	**610 to approximately 750nm**

Table 1. Visible spectrum broken up into the approximate wavelength values[4].

On the other hand, development of organic light emitting diode (OLED) constitute a new and exciting emissive lighting technology. Generally, the luminescent emissions of singlet excitons is the most well-known main mechanism of OLEDs as a result of delocalized pi (π) electrons caused by conjugation over all or part of the molecule[5]. These materials generally have conductivity levels ranging from insulators to conductors, and therefore are considered organic semiconductors. The highest occupied and lowest unoccupied molecular orbitals (HOMO and LUMO) of organic semiconductors are analogous to the valence and conduction bands of inorganic semiconductors. Some OLEDs are already commercialized in the field of display markets due to its advantages such as self-luminous, low cost and easy fabrication, colour selectivity, lightweight, compact and thin device fabrications and flexibility and much more.

In practical applications, exciting electromagnetic radiation such as ultraviolet (UV) radiation is absorbed by the activator ion or sensitizer (second kind of impurity) ions, raising it to an excited state. The excited state returns to the ground state with emission of radiation, in this case by emission of visible wavelength which is commonly used in phosphor-converted UV-LEDs. However, not every exciton is converted to emission radiation due to non-radiative recombination, which vibrates the host lattice[2,4].

Hence, the quantum efficiency, q, which is defined as the ratio of the number of emitted photons to the number of absorbed photons, and in most cases is equal to the ratio of the measured lifetime to the radiative lifetime of a given level. In most cases, it is equal to the ratio of the measured lifetime to the radiative lifetime of a given level[2].

For more technical aspect, two types of quantum efficiency exist, where the internal quantum efficiency (η_0) is how much photons are absorbed by the phosphor converting into luminescence, and external quantum efficiency (η_i) is defined as the ratio of the number of photons of the emitted light to that of the incident light on a phosphor[4].

$$\boldsymbol{\eta_0} = \frac{\int \boldsymbol{\lambda \cdot P(\lambda) d\lambda}}{\int \boldsymbol{\lambda \cdot E(\lambda) d\lambda}}$$

$$\boldsymbol{\eta_i} = \frac{\int \boldsymbol{\lambda \cdot P(\lambda) d\lambda}}{\int \boldsymbol{\lambda\{E(\lambda) - R(\lambda)\} d\lambda}}$$

1.1.1. UV-Light Emitting Diodes

In lighting technology, conventional incandescent light bulbs are still in use, but due to its optical inefficiency as well as the use of toxic mercury, research and development of transition in new lighting technology such as LEDs are highly investigated due to its advantages, including high colour rendering index with different phosphor materials, high luminous efficiency, and stable light colour that are almost independent of the changed current, and exclusion of toxic materials.

According to the relevant literature[6], most of such UV-LEDs devices use inorganic phosphors, which are arranged in Table 2. As presented in Table 2, the intensity, width, durability and thermal quenching of commercial phosphors for UV-LED chip is shown. However, some existing phosphors such as sulphide phosphors do not have chemical stability or thermal stability under either highly applied current or electrical field. In contrast, oxide phosphors show better stability over the sulphides due to their low outgassing and their ability to endure high electron beam current. Moreover, use of non-rare-earth material can additionally diminish the production cost.

Generally, there are three different methods to produce white emission colour by rendering with different phosphor materials, which is ascribed using the schematic diagram in Figure 2. In a single phosphor system, blue LED and yellow phosphor are used to create white emission of light. Similarly in multi phosphor system, red and green phosphors are used with blue LED system to produce white light. Lastly, UV source can also be combined with UV excited red, green, and blue (primary colour) phosphors to produce white light emission.

UV-LED technology is relatively new, but is rapidly emerging to be a viable alternative light source due to significant cost, energy, and space saving compared to alternate technologies. Moreover, it can provide tight beam angle and uniform beam patterns that can be focused directly where it is required[7]. Hence, the development of UV-excited oxide phosphor material will be one of the key challenging technologies to be developed.

LED	Phosphor	Chemical Composition	Emission Characteristics			
			Intensity	Width	Durability	Thermal Quenching
UV-LED	**Blue**	$(Sr,Ca,Ba,Mg)_{10}(PO_4)_6Cl_2/Eu$	O	Narrow	O	△
		$(Ba,Sr)MgAl_{10}O_{17}/Eu$	O	Middle	O	O
		$(Sr,Ba)_3MgSi_2O_8/Eu$	O	Narrow	△	△
	Green	$SrGa_2S_4/Eu$	O	Middle	X	X
		β-sialon/Eu	O	Middle	O	O
		$SrSi_2O_2N_2/Eu$	O	Middle	O	O
		$Ba_3Si_6O_{12}N_2/Eu$	O	Middle	O	O
		$BaMgAl_{10}O_{17}/Eu,Mn$	O	Narrow	O	O
		$SrAl_2O_4/Eu$	△	Broad	△	△
	Red	(Sr,Ca)S/Eu	O	Broad	X	X
		$(Ca,Sr)_2Si_5N_8/Eu$	△	Broad	△	△
		$CaAlSiN_3/Eu$	O	Broad	O	O
		La_2O_2S/Eu	△	Narrow	△	△
		$3.5MgO{\cdot}3\ 0.5MgF_2{\cdot}3\ GeO_2/Mn$	△	Narrow	O	O
		$(Sr,Ca,Ba,Mg)_{10}(PO_4)_6Cl_2/Eu,Mn$	△	Broad	O	O
		$Ba_3MgSi_2O_8/Eu,Mn$	O	Broad	△	△

Table 2. Examples of white LEDs that incorporate UV-LEDs excitable phosphors[6].

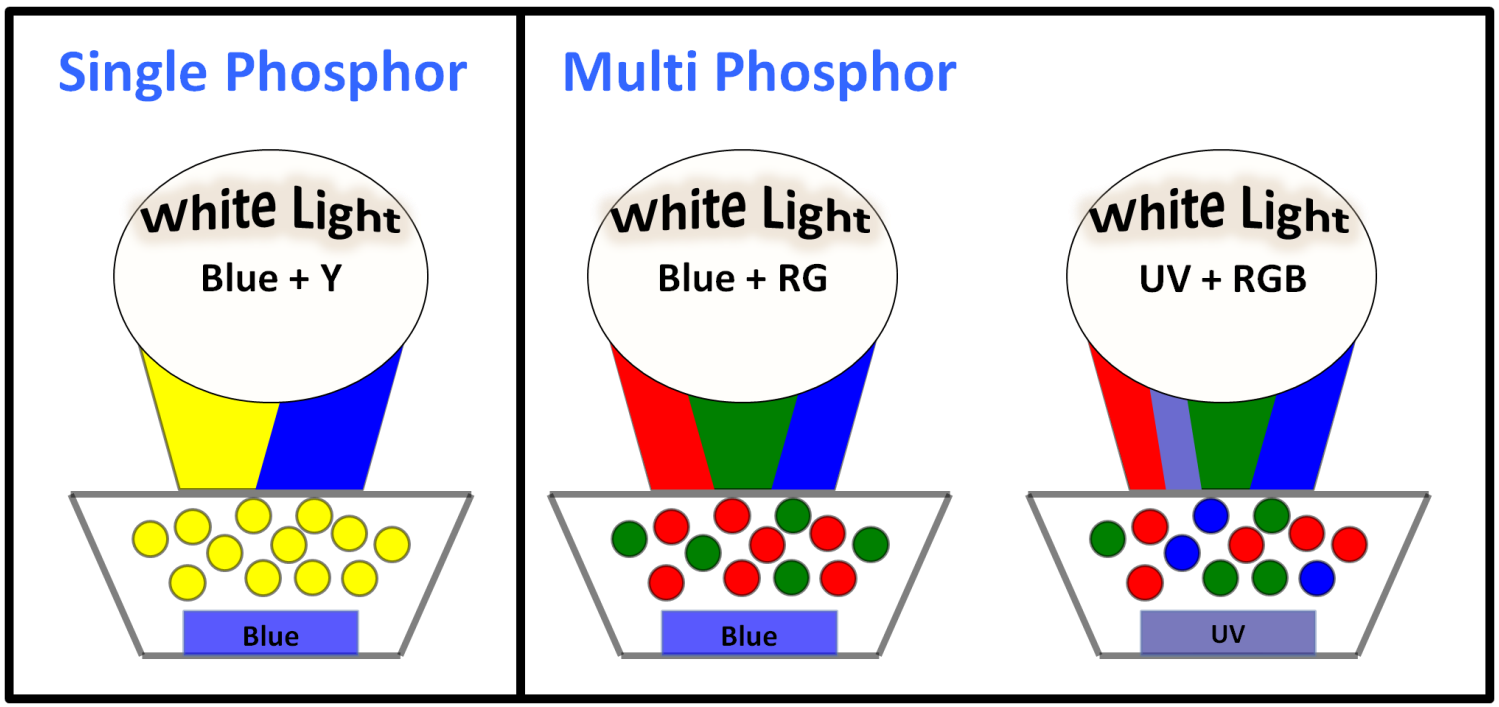

Figure 2. Schematic diagram of Blue and UV-LEDs chip and multi phosphor systems.

1.2. Current study on Zinc Gallate ($ZnGa_2O_4$)

Although there has been several reports related to Zinc gallate ($ZnGa_2O_4$) spinel system, it was in 1991, Itoh et al[8] was one of the first to report on $ZnGa_2O_4$ spinel as a new phosphor system. The spinel, with the general formula AB_2O_4, crystallizes in the normal spinel structure that has FCC close-packed of the cubic spinel structure and like most of other spinels it belongs to Fd3m(O_h^7; No. 227 in the *International tables, 2006*) that can be thought of as a combination of rock salt and zinc blend (Figure 3). The compound of stoichiometry AB_2O_4 in which cations A = Zn^{2+} and B = Ga^{3+}, respectively ZnO and Ga_2O_3 forming spinel. The general coordination of Zn^{2+} and Ga^{3+} ions which specified in international table is shown in Table 3.

The symmetry of each ion usually depends on the atmosphere in which $ZnGa_2O_4$ is heat-treated. Generally, in reducing atmosphere, there is the formation of oxygen vacancies (V_O^*) at tetrahedral or octahedral sites. However, the spinel material exhibits excellent stability and cubic symmetry in spite of the fact that these vacancies will result distortion. This is because spinel structures have the ability to accept structural vacancies, thus forming a defect solid solution while remaining as single phase. The unit cell of $ZnGa_2O_4$ contains Zn^{2+} located at 1/8 of tetrahedral sites and Ga^{3+} located at 1/2 of octahedral sites surrounded by 4 oxygen ions and 6 oxygen ions respectively, and lastly oxygen atoms are located at (u,u,u) position where u indicates the internal parameter[9].

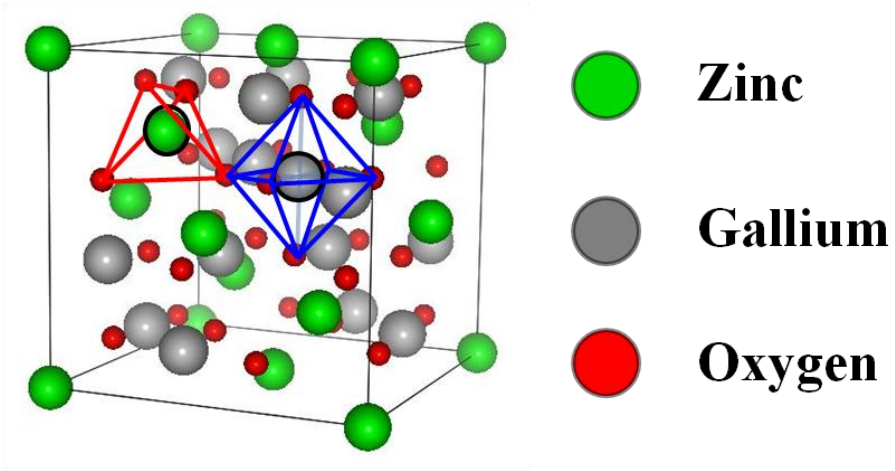

Figure 3. Crystal structure of spinel cubic $ZnGa_2O_4$.

Zn^{2+} ions Tetrahedral Symmetry	000	$\frac{1}{2}\frac{1}{2}0$	$\frac{1}{2}0\frac{1}{2}$	$0\frac{1}{2}\frac{1}{2}$
	$\frac{1}{4}\frac{1}{4}\frac{1}{4}$	$\frac{3}{4}\frac{3}{4}\frac{1}{4}$	$\frac{3}{4}\frac{1}{4}\frac{3}{4}$	$\frac{1}{4}\frac{3}{4}\frac{3}{4}$
Ga^{3+} ions Octahedral Symmetry	$\frac{5}{8}\frac{5}{8}\frac{5}{8}$	$\frac{9}{8}\frac{9}{8}\frac{5}{8}$	$\frac{9}{8}\frac{5}{8}\frac{9}{8}$	$\frac{5}{8}\frac{9}{8}\frac{9}{8}$
	$\frac{7}{8}\frac{7}{8}\frac{5}{8}$	$\frac{11}{8}\frac{11}{8}\frac{5}{8}$	$\frac{11}{8}\frac{7}{8}\frac{9}{8}$	$\frac{7}{8}\frac{11}{8}\frac{9}{8}$
	$\frac{7}{8}\frac{5}{8}\frac{7}{8}$	$\frac{11}{8}\frac{9}{8}\frac{7}{8}$	$\frac{11}{8}\frac{5}{8}\frac{11}{8}$	$\frac{7}{8}\frac{9}{8}\frac{11}{8}$
	$\frac{5}{8}\frac{7}{8}\frac{7}{8}$	$\frac{9}{8}\frac{11}{8}\frac{7}{8}$	$\frac{9}{8}\frac{7}{8}\frac{11}{8}$	$\frac{5}{8}\frac{11}{8}\frac{11}{8}$

Table 3. The general coordinates for the Zn^{2+} and Ga^{3+} ions, specified in the international table.

Recently, the n-type semiconducting $ZnGa_2O_4$ which has an optical band gap of ~ 4.4 – 5.2eV[10,11] has been intensively investigated due to potential application as materials for low voltage field emission displays (FEDs), electro-luminescent devices (ELDs), vacuum fluorescent displays (VFDs), thin-film electroluminescent displays, mechano-optical stress sensors, and stress imaging devices[12,13]. It has an interesting physical and chemical property which exhibits higher chemical stability under high electric field and strong electron bombardment compared to the conventional sulphide based phosphors where degradation has been the major problem[12]. Generally, $ZnGa_2O_4$ emits blue emission due to a transition via a self-activation centre under UV or low voltage electron excitations [10,11,12,13], where self-activation centre of the octahedral Ga-O group in the spinel lattices and the Ga^{3+} ions combine with UV-generated free electrons produced in oxygen vacancies plays the major role in the luminescent mechanism.

On the other hand from literature, $ZnGa_2O_4$ can shift in the emission wavelength into the different regions of the visible spectrum by suitably doping it with transition metals or rare-earth elements. $ZnGa_2O_4$ emits green when doped with manganese (Mn^{2+}) terbium (Tb^{3+}) or thulium (Tm^{3+})[14]. Red emission is achieved by doping with cobalt (Co^{2+}), chromium (Cr^{3+}), and europium (Eu^{3+})[15] producing all RGB primary colours.

Also, our recent laboratory research by J.H. Lim et al[16] reported white emission produced by titanium (Ti) doped $MgAl_2O_4$ spinel material which is in contrast to the blue emission from most Ti-doped single crystal of $MgAl_2O_4$ which may be applicable to other spinel system.

Moreover, there are some reports stating that white long lasting emission was recently achieved by doping with bismuth (Bi^{3+}) by Y. Zhuang et al[17], as well as achievement of red long-persistent luminescent properties with $ZnGa_2(Ge,Sn)O_4:Cr^{3+}$ by Mathieu Allix et al[18]. It should be noted that doping impurities on $ZnGa_2O_4$ is still interesting for phosphor material, but also, there are still remaining potential for other applications as well. Wenli Zhou et al[19] has recently reported the synthesis of porous $ZnGa_2O_4$ prisms which can be applied in optoelectronic, catalytic, sensing, and drug-delivery systems. Moreover, various shape controls for different applications have been reported from simple nanocrystals, colloidal nanocrystals for biological applications to nanowire arrays for FED applications by modifying the synthesis route[20].

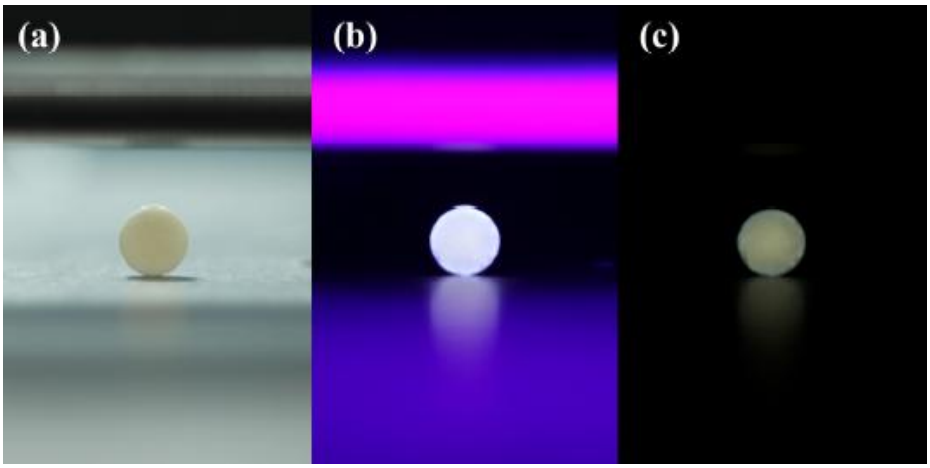

Figure 4. photograph images of the ZGO-Bi sample in nature light (a), under (b) and after stopping (c) excitation of an UV lamp in a dark room[17].

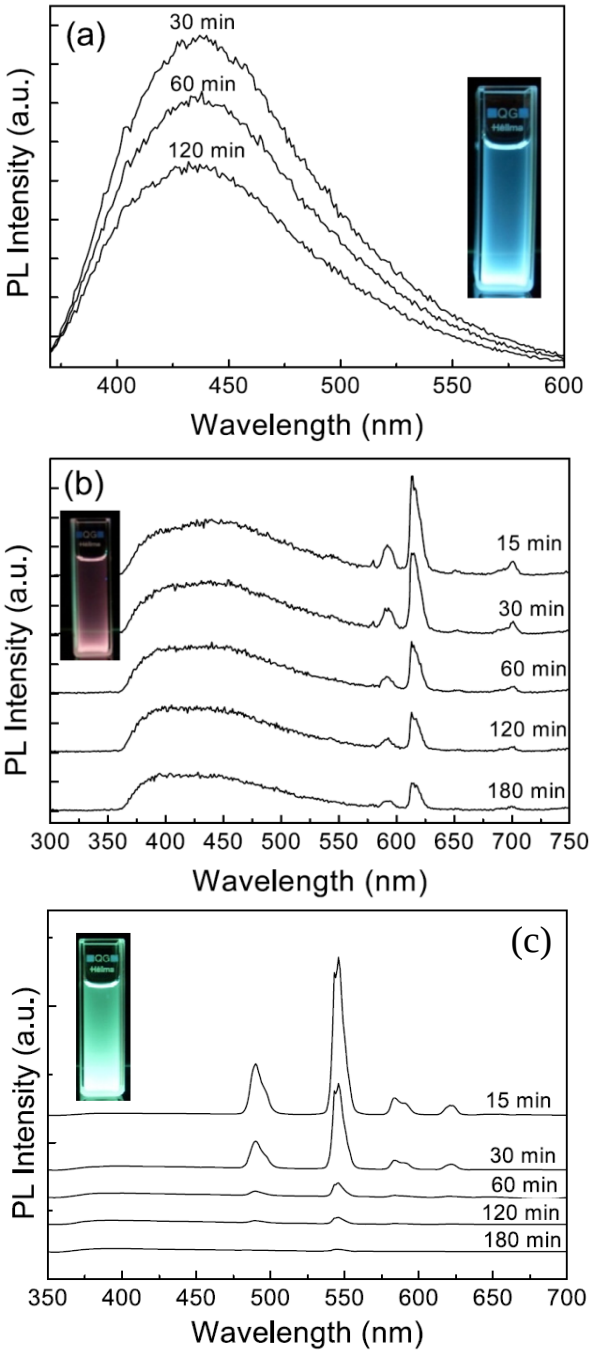

Figure 5. (a) PL emission spectra of $ZnGa_2O_4$, (b) $ZnGa_{1.8}O_4:Eu_{0.2}$ and (c) $ZnGa_{1.8}O_4:Tb_{0.2}$ with an excitation wavelength of 270 nm[21].

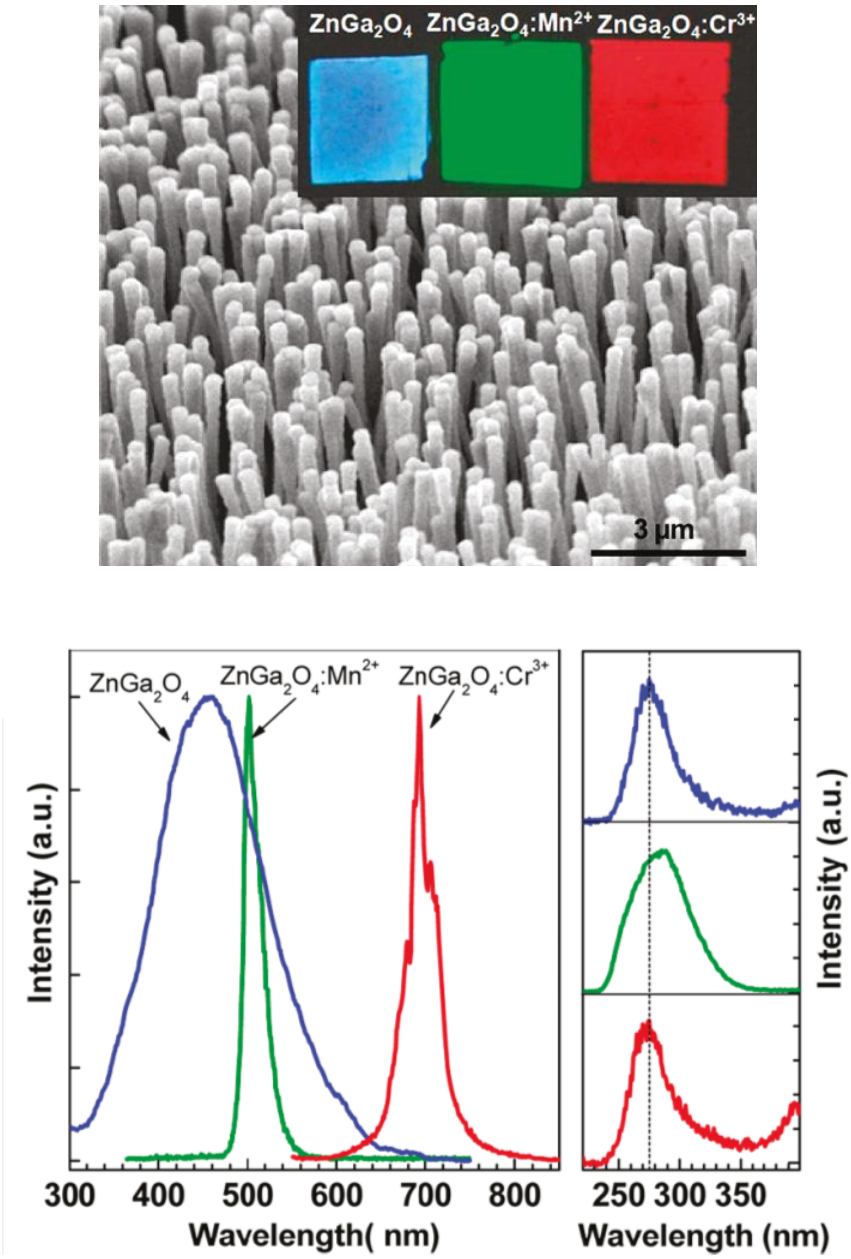

Figure 6. Digital image of (Top figure from left to right) undoped $ZnGa_2O_4$, $ZnGa_2O_4$:Mn^{2+}, and $ZnGa_2O_4$:Cr^{3+} nanowire arrays grown on Si substrates. Photoluminescence spectrum of the samples in panel (Bottom figure) under a 254nm UV lamp irradiation of same nanowire arrays respectively[22].

1.3. Nanomaterials

According to the European commission on 18th of October 2011, a nanomaterials means '*A natural, incidental or manufactured material containing particles, in an unbound state or as an aggregate or as an agglomerate and where, for 50% or more of the particles in the number size distribution, one or more external dimensions is in the size range 1nm – 100nm*'. Many researchers have attempted to produce nanosized phosphor, due to their unique physical, chemical and luminescence properties and their potential applications in fields such as biology[23,24,25]. Hundreds of products containing nanomaterials are already in use of our daily life. Examples include batteries, bio-compatible materials, and optical devices etc. nanomaterials can be classified based on dimension namely 0D, 1D, 2D and 3D[26] as shown in the Figure 7. However, the new materials may cause some risk to the environment and raise health and safety concerns as for the use of toxic precursor and synthesis method. Nevertheless, the properties derived from nanosized including the chemical reactivity of materials as well as their mechanical, optical, electrical and magnetic properties, are irresistibly attractive, and hence the investigation regarding the nanomaterials will enhance the field of many applications.

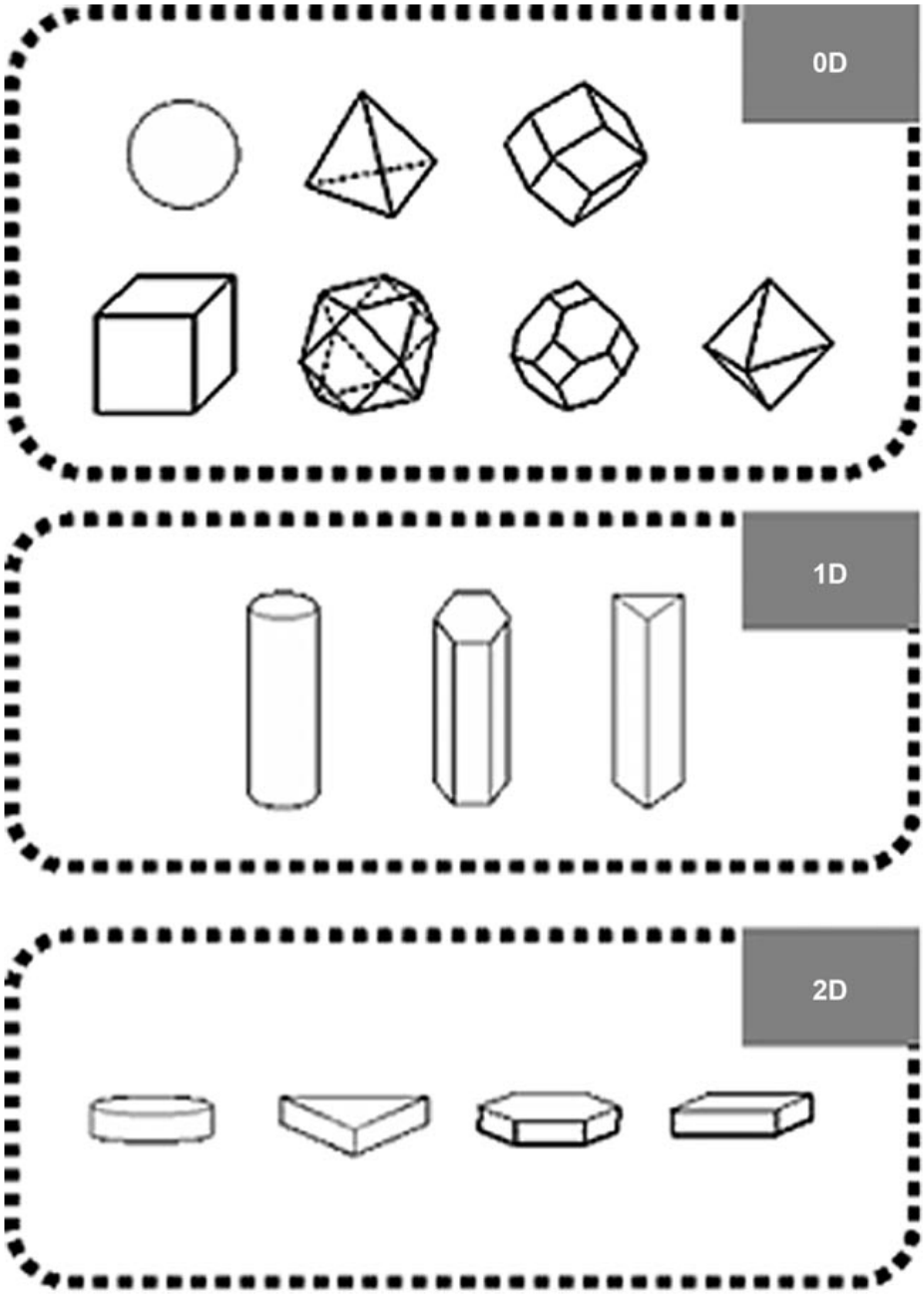

Figure 7. Basic motifs of inorganic nanocrystals: 0D spheres, cubes, and polyhedrons; 1D rods and wires; 2D discs, prisms, and plates[26].

1.4. Synthesis of Phosphor Materials

Various methods have been proposed to synthesize inorganic phosphors. The selection of which method to be used for phosphor fabrication has to be very carefully selected since the particle size, morphology, microstructure, luminescence properties and quantum efficiencies are strongly affected by synthetic method. Presently, the most extensively used ones including solid state reaction and wet chemical methods are described as follow.

1.4.1. Solid State Reaction Method

The solid state synthesis method is one of the most widely used techniques especially for a mass production due to its simple and straightforward preparation. Generally, single cation ceramic or oxide powders are used as precursor, which are mixed together and heated to high temperature to promote interdiffusion and the eventual development of a single phase[12]. However, this method is known to introduce impurity phases from unreacted intermediate, but also due to the high temperatures used during production, non-stoichiometric amounts of precursor may required to compensate for losses arising from differences in volatility[13]. Furthermore, the average particle size of the phosphors prepared by this method is often larger than 5μm[27], making light scattering an issue for integration with a near UV (nUV) chip.

1.4.2. Sol-Gel / Pechini Method

Since the development of sol-gel process (named after its American inventor, Maggio Pechini), there has been an intense level of research on developing luminescent and other material as well as modifying this method. The process include, metal oxide with appropriate molar ratio are dissolved in an acid solution. Chelating agent is then added along with cross-linking agents. The solution is generally heated at 150 - 250℃ to allow the chelating agent to polymerize, or to form a large cross-linking network, producing a transparent gel. Calcination of this gel will eventually produce an oxide[28]. The method is appropriate for producing nano-particles due to particle size being extremely small, typically 20 to 50nm[29]. Although there is a drawback of agglomeration, modification of the method has been proven to prevent from this effect[27].

1.4.3. Combustion Method

Combustion method is another form of Pechini process which rapidly produces multi-constituent oxides. The method is similar, but involves igniting an aqueous solution of dissolved metal nitrates and a fuel (e.g. urea, glycine, carbohydrazide) at a temperature lower than 500℃, allowing the highly exothermic and oxidative reaction of sudden temperature of more than 1200℃ with very short reaction time[27]. Because of this short time of reaction, nanocrystalline powders are produced, but again agglomeration is another issue of this method.

1.4.4. Co-Precipitation method

This method is widely used to fabricate oxide and (oxy)fluoride-based phosphors[30]. Generally, metal nitrates, acetate and chlorides precursors are dissolved in a solvent (e.g. water) followed by addition of precipitating agents. Since the precursors should dissolve and precipitate should not, the solubility of both the precipitates and precursors in the solvent should be confirmed before starting the procedure. Once the precipitates are formed, it is separated by filtering or centrifuging and heated to decompose hydroxide or carbonate that was previously formed during precipitation. The powder is then annealed at high temperature to crystallize the powder. The product consists of small particle size, homogeneously distributed activator ions as well as uniform and narrow size distributions[27]. However, the preparation may be difficult during the use of chloride-based phosphor, due to the dissolution of precipitates (metal chloride) in the solvent[28].

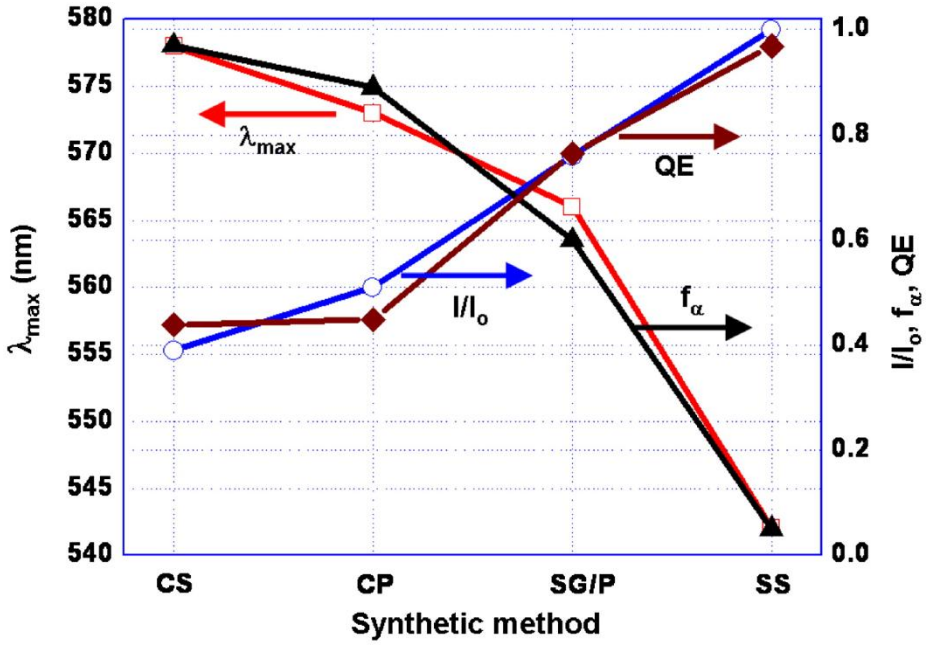

Figure 8. The effect of synthesis method on the luminescence properties of $Sr_2SiO_4:Eu^{2+}$; CS=combustion synthesis, CP=co-precipitation, SG/P=sol-gel/Pechini, SS=solid state[31].

Figure 8 represents the quantum efficiency prepared by four different synthesis methods (combustion, co-precipitation, sol-gel/Pechini, and solid state reaction) by J.K. Han, et al[31]. Of course, not every phosphor system is expected to follow the exact tendency as seen in Figure 8, the result of each different synthesis method were carefully considered and consulted for the current dissertation. Although there exist a number of other synthetic methods, by carefully analyzing the pros and cons from an engineering perspective, modification among these synthetic methods are expected to give interesting results. Table 1 was also considered which provide a general idea of properties achieved using different methods.

Synthesis method	Solid State Reaction(SS)	Sol Gel/Pechini (SG/P)	Co-Precipitation (CP)	Combustion (CS)
Particle Size	**> 5µm**	**10 nm - 2µm**	**10nm - 1µm**	**500nm - 2µm**
Particle Size distribution	**Narrow – Broad**	**Narrow**	**Narrow**	**Medium**
Morphological Control	**Poor – Good**	**Medium**	**Very Good**	**Poor**
Purity	**Poor – Very Good**	**Good**	**Medium**	**Medium – Good**
Cost	**Low**	**Medium**	**Medium**	**Low – Medium**
Synthesis time	**Short – Long**	**Medium**	**Medium**	**Short**
Suitable phosphors	**All compounds**	**All compounds except nitrides**	**Oxides and fluorides**	**All compounds except nitrides**
Limitations	**- Extensive grinding and milling required**	**- Requires a soluble precursor - Carbon contamination - Difficult to obtain nitrides, sulphides, and other non-oxides materials**	**- Requires a soluble precursors - Difficult to obtain nitrides**	**- Requires a soluble precursor - Carbon contamination - Difficult to obtain nitrides**

Table 4. Summary of synthesis methods: particle size, morphology control, chemical homogeneity, cost, time, suitable phosphors and limitations[27].

1.5. Objective of the Study

In this dissertation, the optical properties of nano $ZnGa_2O_4$ produced from liquid-phase combustion method were mainly investigated with comparison to the bulk system. Along with luminescent features, dependency of particle sizes with difference in temperatures was studied. Moreover, transitional metals, chromium and titanium, were doped into the host material to characterize the effect of emission colour.

Last of all, excess organic impurity was intentionally introduced in $ZnGa_2O_4$ by synthesizing with a non-stoichiometrically balanced system. The luminescence of this organic impurity containing $ZnGa_2O_4$ was also characterized in similar manner. The DV-Xα calculation was attempted and its result was referred to interpret the emission mechanism. The calculated energy diagrams and density of state (DOS) closely converged with the main emission mechanism of the actual experimental data, showing good reliability of the method. However, for a more precise calculation, further work such as addition of oxygen vacancy must be included which is in progress and therefore the result is included in the appendix section.

Chapter 2. Experimental Methods

2.1. Material Synthesis of Bulk $ZnGa_2O_4$

$ZnGa_2O_4$ spinel compositions were synthesized by solid state reaction using one to one stoichiometry of pure ZnO (99.9%, Sigma-Aldrich) and pure Ga_2O_3 (99.995%, Cerac) as starting materials. ZnO and Ga_2O_3 were wet mixed in a Nalgene bottle using ethanol and YSZ ball milled at 200rpm for 20 hours to ensure homogeneously mixed starting materials. The ball to powder ratio was 30:1. After drying the solution in an oven at 100℃ for 24 hours, the dried powder was sieved through a 250 mesh to eliminate any large agglomerated powder. Lastly, powder was heat-treated at 1000℃ for 12 hours in ambient atmosphere. For comparison to the nanosized material, the synthesized powder was grinded in an agate mortar for powder characterization.

2.2. Material Synthesis of Nano $ZnGa_2O_4$

Nano $ZnGa_2O_4$ spinel compositions were synthesized using liquid-phase combustion method involving oxidizing and reducing agent. 1:2 molar ratio of $Zn(NO_3)_2 \cdot 6H_2O$ (98%, Sigma-Aldrich) and $Ga(NO_3)_3 \cdot xH_2O$ (99.9%, Sigma-Aldrich) were used as precursor and 0.02 mole fraction for both $Cr(NO_3)_3 \cdot 9H_2O$ (99%, Sigma-Aldrich) and $TiO[CH_3COCH=C(O^-)CH_3]_2$ (90%, Sigma-Aldrich) were used for dopants. Mixture between zinc nitrate and gallium nitrate (oxidizing agent) were mixed in DI water with magnetic stirring in an alumina crucible. Once precursors were all dissolved, urea, $CO(NH_2)_2$, were added as fuel (reducing agent) according to the stoichiometrically balanced system ascribed by S.R. Jain et al[32] and stirred until all materials are dissolved and homogeneously mixed. After dissolution, the magnetic stirrer is taken out then heated on a hot plate at 250℃ until excess water were all evaporated, followed by formation of gel-like form. The alumina crucible containing gel is then moved to a box furnace and heat-treated at 300, 500, 700 and 1000℃ for 1 hour for synthesis of $ZnGa_2O_4$ spinel powder. Synthesized powders were grinded in an agate mortar for powder characterization. Schematic diagram of material synthesization of nano $ZnGa_2O_4$ is represented in Figure 9.

2.3. Material Synthesis of Organic impurity containing $ZnGa_2O_4$

Organic impurities were intentionally introduced in $ZnGa_2O_4$ spinel using the same experimental procedure, liquid-phase combustion method. Similar experimental procedure to the previous nano $ZnGa_2O_4$ was employed except non-stoichiometrically balanced precursors were chosen between oxidizing and reducing agents. In this experiment, zinc acetate dihydrate, $Zn(CH_3COO)_2 \cdot 2H_2O$, was used instead of zinc nitrate hexahydrate, where zinc acetate dehydrate is also a reducing agent like urea breaking the stoichiometry of redox reaction. Exactly same amount of molar ratio to the previous experiment were taken. Zinc acetate dihydrate and gallium nitrate were dissolved and homogeneously mixed in DI water by using the magnetic stirrer. After dissolution, urea was added as a reducing agent until further dissolution. The magnetic stirrer was taken out after full dissolution of the precursor, then heated on a hot plate at 250℃ until excess water was fully evaporated, which was followed by formation of gel-like state. The alumina crucible containing gel is then moved to a box furnace and heat-treated at 300, 500, 700, 1000℃ for 1h, denoted as AN(300) to AN(1000), to observe the temperature dependency on the product. All synthesized powders were grinded in an agate mortar for powder characterization.

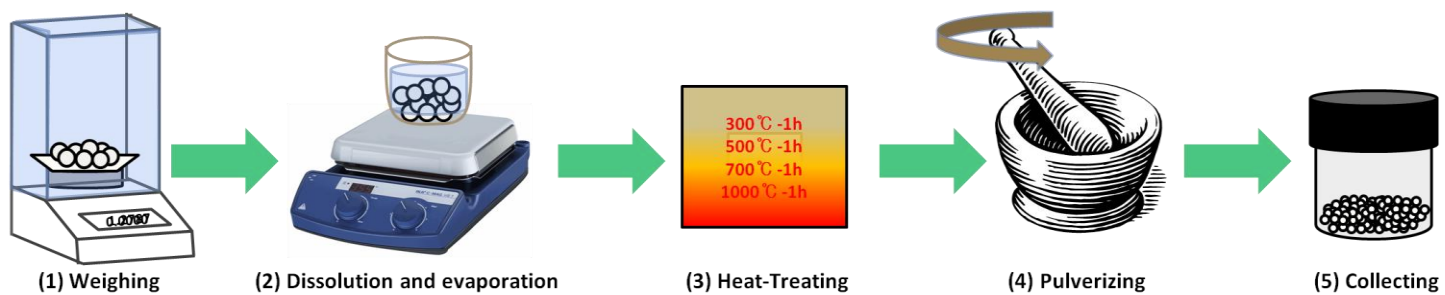

Figure 9. A schematic diagram of synthesization of nano $ZnGa_2O_4$.

2.4. Characterization Methods

Crystal structure of $ZnGa_2O_4$ measurement was performed on Laboratory X-ray powder diffraction (XRD) on a Rigaku D-max 2500 (CuKα radiation) equipped with Vantec-1 linear detector. Data was collected between 20° and 80° (2θ) at room temperature with a 0.0164° step size. The distribution of dopant ions over the tetrahedral or octahedral sites or both in the spinel structure was calculated by Rietveld refinement of the XRD patterns (HighScore plus programme). The calculation of crystallite sizes were performed based on Scherrer's method.

High Resolution Transmission Electron Microscopy (HRTEM) data was collected on a JEOL-3000F microscope fitted with an Oxford energy Dispersive Spectrometry (EDS) analyzer. The powder samples were dispersed in acetone and mixed by ultrasonication, and a drop of the solution with the small crystallites in suspension was deposited onto carbon-coated copper grid. The morphology and size of powder samples heat-treated at 1000℃ for 1h were collected using Field Emission Scanning Electron Microscopy (FE-SEM) data collected on a JEOL, JSM-6330F microscope. The powder samples were placed on a carbon tape.

The excitation and emission spectra were recorded at room temperature using PTI spectrofluorometer equipped with a filter wavelength range between 400nm to 800nm. High resolution spectra were recorded by reducing the entrance and exit slits to 0.5nm.

The energy diagram of the spinel was obtained using the first-principle software, Discrete Variational Xα (DV-Xα) molecular orbital method. The difference between calculated and experimental results were compared and

interpreted. With DV-Xα, various physical properties can be calculated through the integration of discrete variation. The molecular orbital result was explained by Mulliken method. The final values of electrical densities were calculated until the result converges to initial value assuming before the numerical basis function was obtained[33]. This method approximates the exchange correlation interaction with the Xα potential proposed by Slater and numerically solves the Schrödinger equation using the Hartree-Fock-Slater method. No restriction was imposed on the form of the basis functions because the calculation was conducted numerically[34, 35]. There was no consideration in the calculation on the electron vibrations (modes), corresponding relaxation and nuclear transition in the excited state. Even if this causes errors in absorption and emission wavelength, still, this calculation method is believed to provide meaningful insights into emission mechanisms based on band-to-band transition. The cluster model used for the calculation was $[Zn_6Ga_{19}O_{88}]^{-7}$, which showed the convergence of the final values as mentioned above. However, the result was only considered as reference as for more precise calculation oxygen vacancy is majorly required.

Chapter 3. Results and Discussion

3.1. Spinel Oxide Phosphor : $ZnGa_2O_4$

3.1.1. Bulk Spinel Oxide: $ZnGa_2O_4$

The structure of normal spinel $ZnGa_2O_4$ belongs to Fd3m (O_h^7; No. 227 in the international tables, 2006). Figure 10 represents the crystal structure of $ZnGa_2O_4$ reproduced by using the Rietveld Highscore Plus programme, where Zn^{2+} ions occupying the eight sites have tetrahedral symmetry, whereas Ga^{3+} ions occupying the sixteen sites have octahedral symmetry. $ZnGa_2O_4$ spinel with doped or undoped phosphors are typically synthesized by solid state reaction between ZnO and Ga_2O_3, where high temperature with several hours of heating is generally required (usually >1000℃)[10].

The Figure 11 represents the powder X-ray diffraction (XRD) patterns of $ZnGa_2O_4$ produced by solid state reaction at 1000℃ for 4hours. XRD patterns were in good agreement with $ZnGa_2O_4$ reference data from JCPDS entry #00-038-1240 with few existing secondary phases. These secondary peaks have been already reported as due to the volatilization of ZnO phase at such high temperature[10], it can intricate the synthesis of exact stoichiometric $ZnGa_2O_4$ as seen in the Figure 11. Although solid state reaction is advantageous as the simplest synthesis route, the resulting product is likely to possess many impurities. To overcome such problem, alternative low temperature routes such as wet chemical approaches were developed by employing metal-organic complexes as precursors, which generally produces nanocrystallite form. Hence, in this work, metal nitrate and urea were used to synthesize stoichiometric nano $ZnGa_2O_4$ phosphor powder with our newly developed

liquid-phase combustion method as this wet chemical method has been reported to be sufficient for the formation of complex oxide phases such as spinel structure with minimized formation of secondary phase[27].

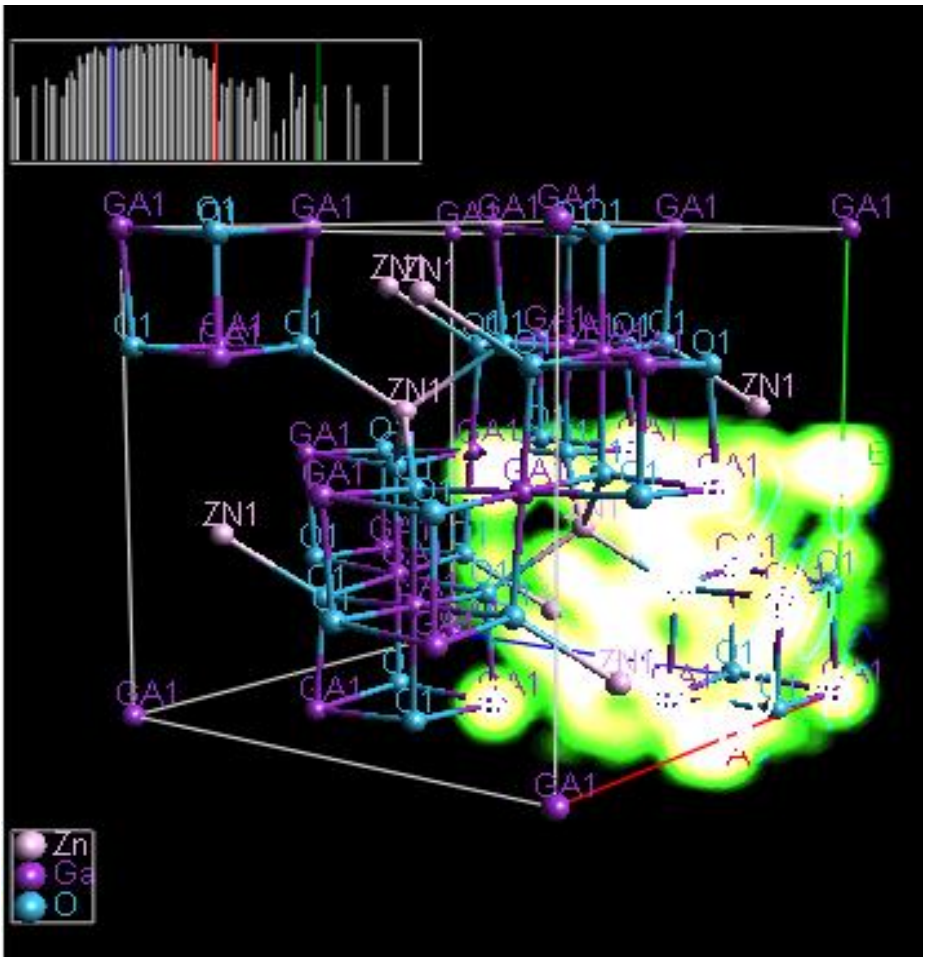

Figure 10. $ZnGa_2O_4$ crystal structure reproduced using Rietveld Highscore Plus.

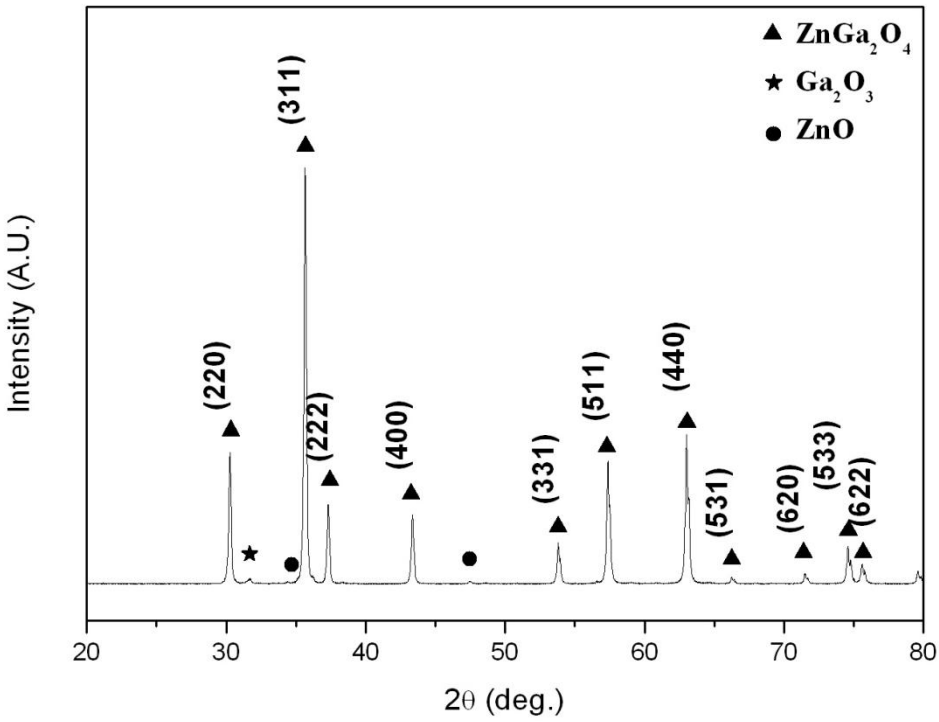

Figure 11. Powder XRD patterns of bulk $ZnGa_2O_4$.

3.1.2. Synthesis of metal oxide through metal-organic precursor

Figure 12 and Figure 13 both illustrates the powder x-ray diffraction (XRD) patterns of each heat-treated precursor materials, zinc nitrate hexahydrate and gallium nitrate hydrate respectively, at different heating temperatures from 500, 700, and 1000℃ for 1h in ambient atmosphere. Formation of ZnO and Ga_2O_3 was expected when precursor was heated at high temperature as degradation of organic materials will leave metal ions to react with the surrounding oxygen to form the most stable phase, metal oxide. From Figure 12, ZnO seems to form readily at any given appropriate temperature, whereas in Figure 13, the formation of Ga_2O_3 only occurred at 700 and 1000℃, suggesting the formation of $ZnGa_2O_4$ at about 700℃, where formation temperature of each metal oxide converges.

However, thermochemistry of the system ascribed by S. R. Jain et al. can be applied to lower the required reaction temperature[32] by the following method. In Fuel-Oxidizer compositions such as metal nitrate with addition of urea (fuel) will act as oxidizing agent and reducing agent respectively. Arand et al. (1980) first reported that urea could be used as reducing agent to remove NO_x by selectively reducing NO_x and there are number of other reagents that can be used as reducing agents. Although ammonia is one of the well known NO_x reducing agents, it has several disadvantages such as pure ammonia can lead to stress corrosion cracking, may explode with a certain proportion to air but most importantly, it is toxic gas and any leakage may cause serious harm to health. On the other hand, urea is non-corrosive and much safer than ammonia[36]. Hence, in this dissertation, urea was naturally chosen as the reducing NO_x in metal nitrate.

Figure 14 and Figure 15 both illustrate the powder XRD patterns of heat-treated precursor materials at 500℃ with addition of different amount of urea. It can be noted that the characteristic of ZnO appears almost in every sample except when the amount of urea is abnormally exceeding the stoichiometry. On the other hand, Ga_2O_3 only appears when the gallium nitrate is stoichiometrically balanced with urea. The broad amorphous like XRD patterns are represented possibly due to small crystallite size but it is more likely because of the existence of organic molecules.

Moreover, Figure 16 illustrates that with exceeding the stoichiometry amount of urea will decrease the crystallinity. Hence, the control of stoichiometry between urea and oxidizer mixture will be critical for a complete removal of NO_x in nitrate through redox reaction, as excess amount will only leave undesirable organic molecules at the surface but deficient amount will result incomplete or very slow rate of reaction as well as requirement of higher reaction temperature. As a consequence, these results indicate the possibility of synthesizing nano $ZnGa_2O_4$ at temperature below 1000℃ with addition of urea.

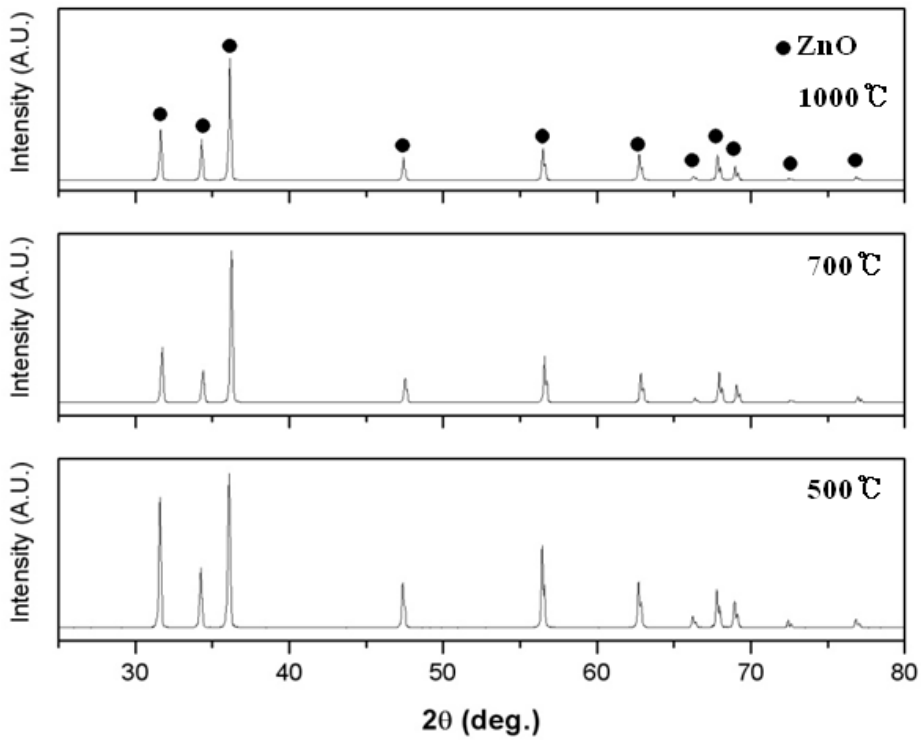

Figure 12. Powder XRD patterns of zinc nitrate heated at different temperature.

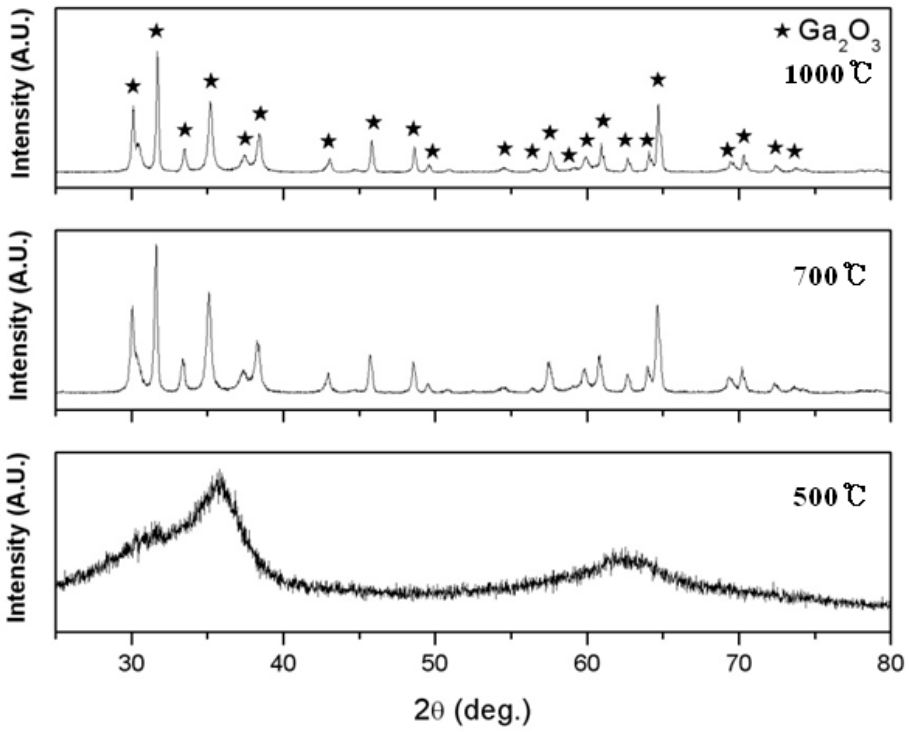

Figure 13. Powder XRD patterns of gallium nitrate heated at different temperatures.

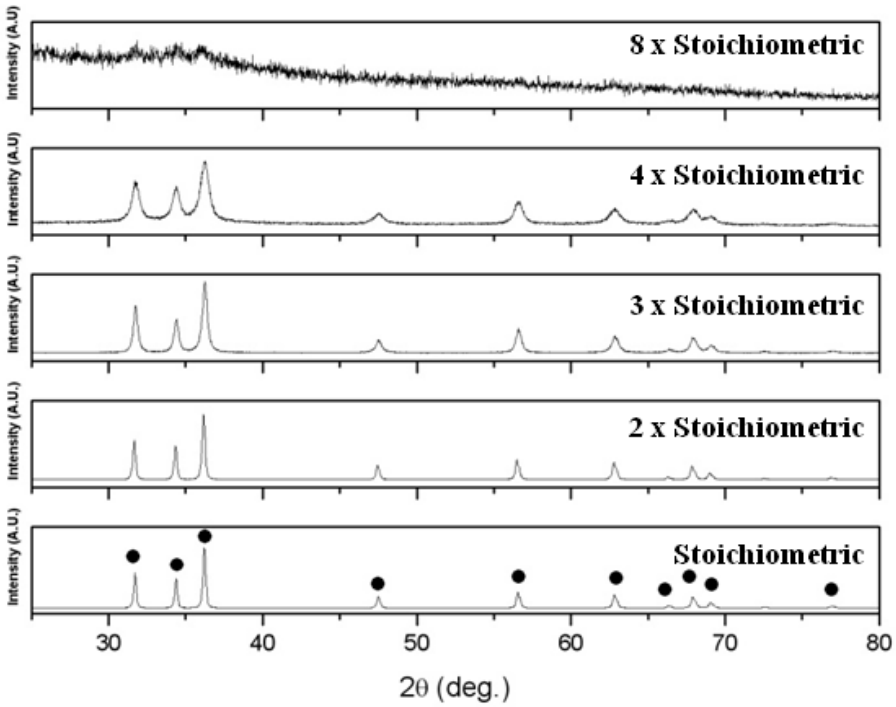

Figure 14. Powder XRD patterns of zinc nitrate with various amount of urea heated at 500℃.

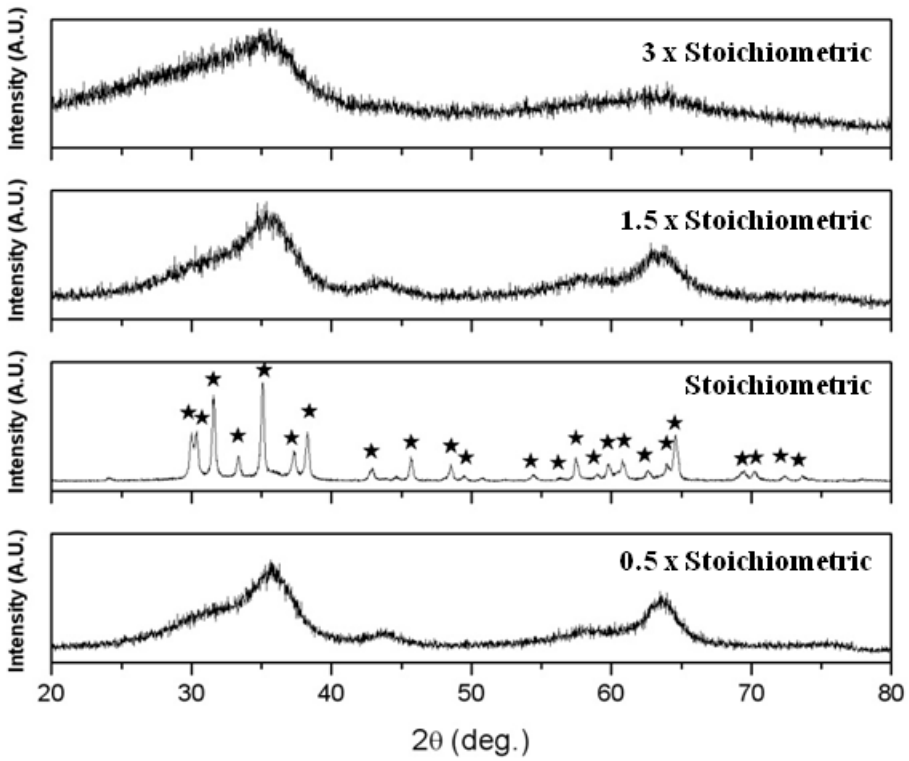

Figure 15. Powder XRD patterns of gallium nitrate with various amount of urea heated at 500℃.

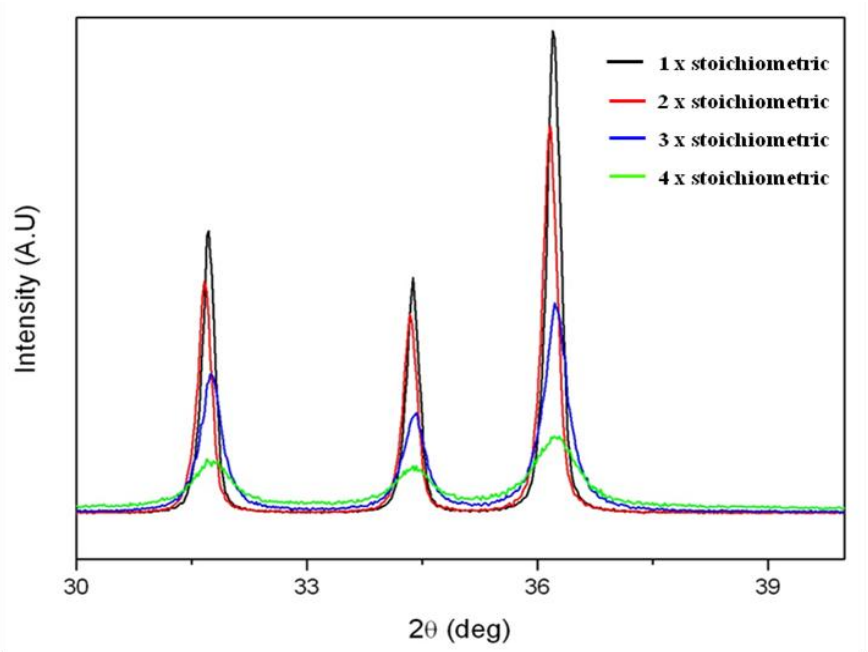

Figure 16. A close observation of powder XRD patterns of zinc nitrate with various amount of urea heated at 500℃.

3.2. Material characterization of nano $ZnGa_2O_4$

3.2.1. Nano spinel oxide: undoped - $ZnGa_2O_4$

Nano $ZnGa_2O_4$ was synthesized through stoichiometrically balanced redox reaction. The powder XRD patterns of $ZnGa_2O_4$ heat-treated at 300, 500, 700, and 1000℃ for 1h are shown in Figure 17(a). The increase in crystallinity with decrease in full width half maximum (FWHM) is observed with higher temperature. Despite significantly broadened peaks with low temperature synthesized sample at 300℃, characteristics of the spinel phase are found in all diffraction peaks which agrees well with the cubic spinel of $ZnGa_2O_4$ from JCPDS entry #00-038-1240 (Figure 17(b)), indicating that a single phase of $ZnGa_2O_4$ was synthesized without any secondary phases such as ZnO or Ga_2O_3. The results also demonstrate the possibility of low temperature synthesis of $ZnGa_2O_4$ by liquid-phase combustion method which is much lower than the conventional solid state reaction.

Figure 18 illustrates the XPS spectra of $ZnGa_2O_4$, and the wide scanning spectrum indicating the existence of Ga, Zn and O elements depicted in Figure 18(a) and no contamination seems to be present other than very low peak from adsorbed carbon is present in the spectra. The fine XPS spectrum in Figure 18(b) reveals $Ga2p_{3/2}$ and $Ga2p_{1/2}$ peaks at 1115.8 and 1142.65 eV, respectively. The gap between the two peaks is 26.85 eV. The fine XPS spectrum of Zn $2p_{3/2}$ and $Zn2p_{1/2}$ peaks at 1019.75 and 1042.9 eV is shown in Figure 18(c), where the gap between two peaks is 23.15 eV. Lastly, the fine XPS spectrum of O 1s at 528.85 eV is illustrated in Figure 18(d). The value and the gap between fine XPS of Ga and Zn all agreed with the reference values[10,37].

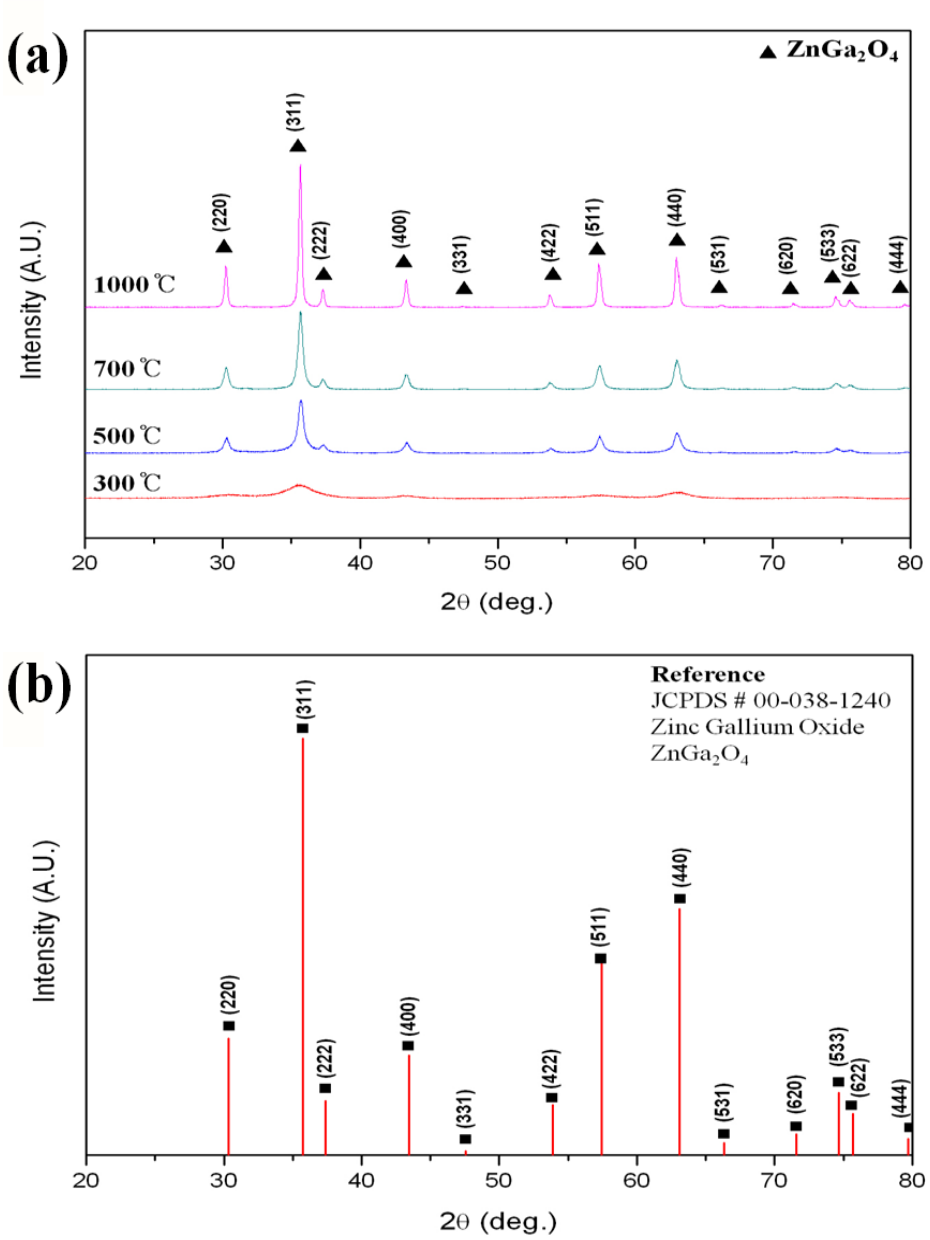

Figure 17. (a) Powder XRD patterns of $ZnGa_2O_4$ prepared by stoichiometrically balanced system heat-treated at various temperature in ambient atmosphere for 1h . (b) XRD patterns of $ZnGa_2O_4$ reference from JCPDS #00-038-1240.

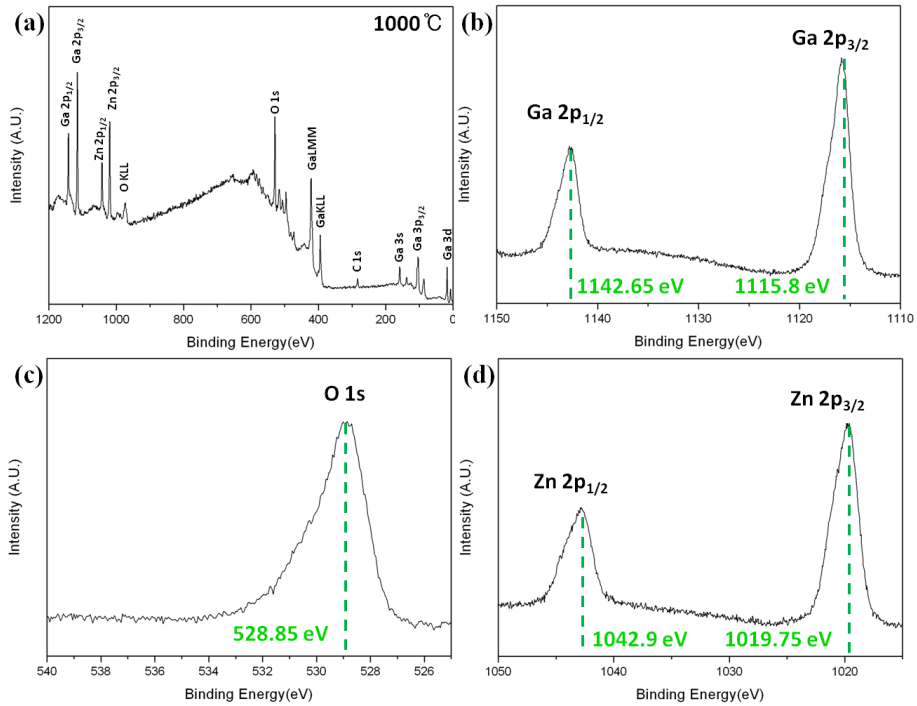

Figure 18. XPS spectra of $ZnGa_2O_4$: (a) wide scanning spectrum and the fine spectra of (b) Ga 2p, (c) Zn 2p, (d) O1s.

3.2.2. Nano spinel oxide : doped - $ZnGa_2O_4$

Figure 19 and Figure 20 shows powder XRD patterns of chromium and titanium-doped $ZnGa_2O_4$ prepared at 500℃ for 1h. All XRD patterns are in good agreement with $ZnGa_2O_4$ reference data of JCPDS entry #00-038-1240 despite the broadened peaks with Ti-doped $ZnGa_2O_4$. Two theta (2θ) values of nanosized doped $ZnGa_2O_4$ are slightly different from the undoped $ZnGa_2O_4$ (illustrated in Figure 19 and Figure 20 bottom) which is due to the difference in ionic radii between substituted ions.

Although no secondary phase was observed from XRD result, additional XPS analysis was carried out to verify the existence of dopants as well as the oxidation state of each ions allowing us to determine which atoms are substituted in $ZnGa_2O_4$. The Figure 21 represents the XPS analysis of Cr-doped $ZnGa_2O_4$. The wide scanning spectrum indicates the existence of Ga, Zn, O and Cr elements depicted in Figure 21(a). Similar to undoped $ZnGa_2O_4$, no other contamination is observable other than very low carbon peak from adsorption. $Ga2p_{3/2}$ and $Ga2p_{1/2}$ peaks at 1115 and 1143 eV are shown in the fine XPS spectrum in Figure 21(b). The gap between two peaks is 27 eV. The fine XPS spectrum of Zn $2p_{3/2}$ and Zn $2p_{1/2}$ peaks at 1019.8 and 1042.9 eV is shown in Figure 21(c), where the gap between two peaks is 23.1 eV. Lastly, the fine XPS spectrum of Cr $2p_{3/2}$ and Cr $2p_{1/2}$ peaks at 574 and 585 eV is shown in Figure 21(d) with the gap difference of 11 eV where this binding energy represents Cr^{3+} trivalent oxidation state. Moreover, all these values and the gap between the fine XPS of Ga and Zn and Cr all agreed with the reference values, suggesting successful synthesis of $ZnGa_2O_4$:Cr^{3+}[22,37].

Lim et al.[16] has recently reported bluish white emission from Ti-doped $MgAl_2O_4$ spinel confirming the existence of both Ti^{3+} and Ti^{4+} ions. XPS was further used to investigate the surface electron state of Ti-doped $ZnGa_2O_4$ prepared at both 500 and 1000℃-1h nanocrystals which is illustrated in Figure 22. Again, the wide spectrum in Figure 22(a and c) show the existence of all Ga, Zn, O and Ti with small contamination of carbon.

Deconvolution of graph was required for both Ti fine XPS spectrum due to broadening of peaks. Sample synthesized at 500℃ (Figure 22 (b) and Figure 22(d)), peaks are positioned at 456.7 and 458.15eV, and with the sample synthesized at 1000℃, peaks are positioned at 456.55 and 458.45eV. According to literature, these peaks are attributed from Ti^{3+} $2p_{3/2}$ and Ti^{4+} $2p_{3/2}$ states respectively[38]. Although the fine spectrum reveals the existence of both Ti^{3+} and Ti^{4+}, but the higher intensity was observed with Ti^{3+} ions which became more obvious with increased synthesis temperature, suggesting the trivalent oxidation state is more favourable state with our host material.

Moreover, because the size difference is very small between gallium (62pm) and titanium (67pm), as well as the stability in charge balance between Ga^{3+} and Ti^{3+}, substitution of Ti^{3+} in Ga^{3+} octahedral position is reasonably the most stable as there will be less strain-stress occurring in the system. Furthermore, slight lower shift in 2θ value in XRD results of doped-$ZnGa_2O_4$ can be explained more clearly. According to Bragg's law, $n\lambda = 2d\sin(\theta)$, where n is an integer, λ is the wavelength of the radiation, d is the spacing of the crystal lattice planes responsible for a particular diffracted beam, and θ is the diffraction angle. According to the published ionic radii data (Los Alamos Laboratory, 2011), Ga = 62pm, Ti = 67pm and Cr = 63pm. Hence, the substitution of Ga^{3+} with Ti^{3+} or Cr^{3+} having larger ionic size will shift into the lower angle of degrees. Moreover, the broadened XRD patterns from Ti-

doped $ZnGa_2O_4$ suggest that the average crystallite size is expected to be much smaller than the other samples.

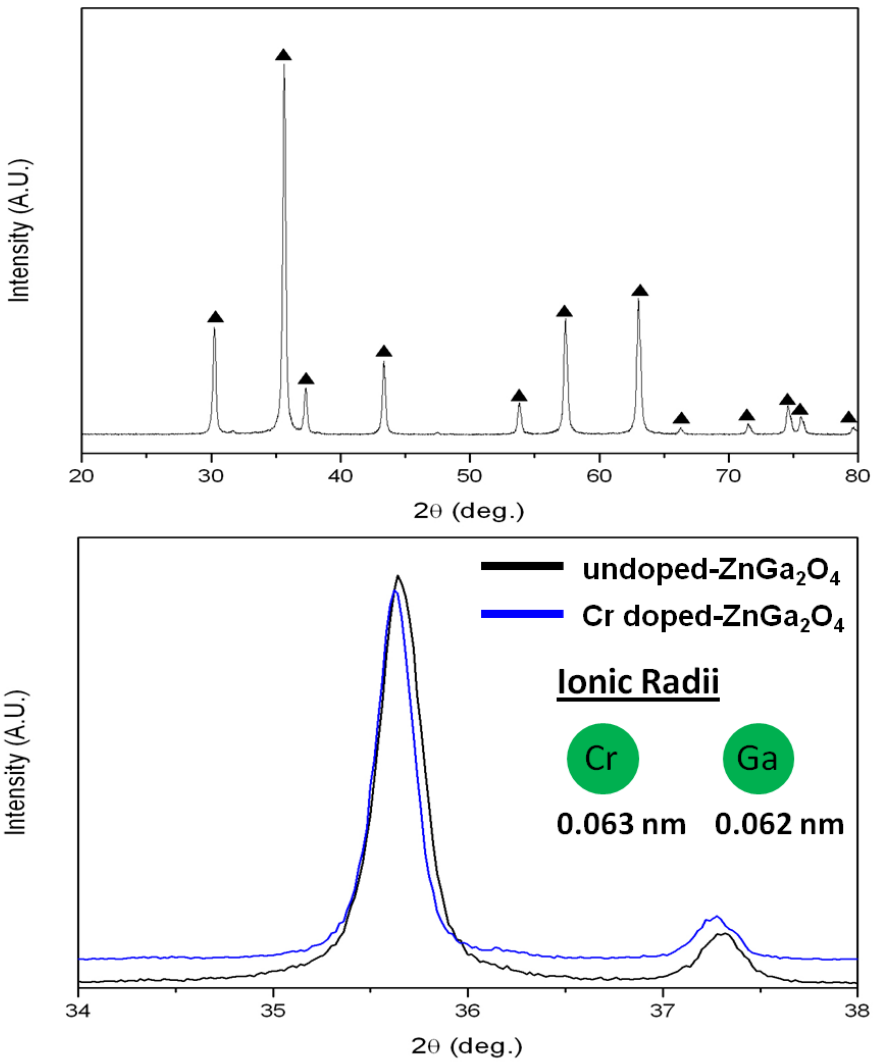

Figure 19. (top) Powder XRD patterns of Cr-doped $ZnGa_2O_4$. (bottom) Close comparison between Cr-doped and undoped $ZnGa_2O_4$.

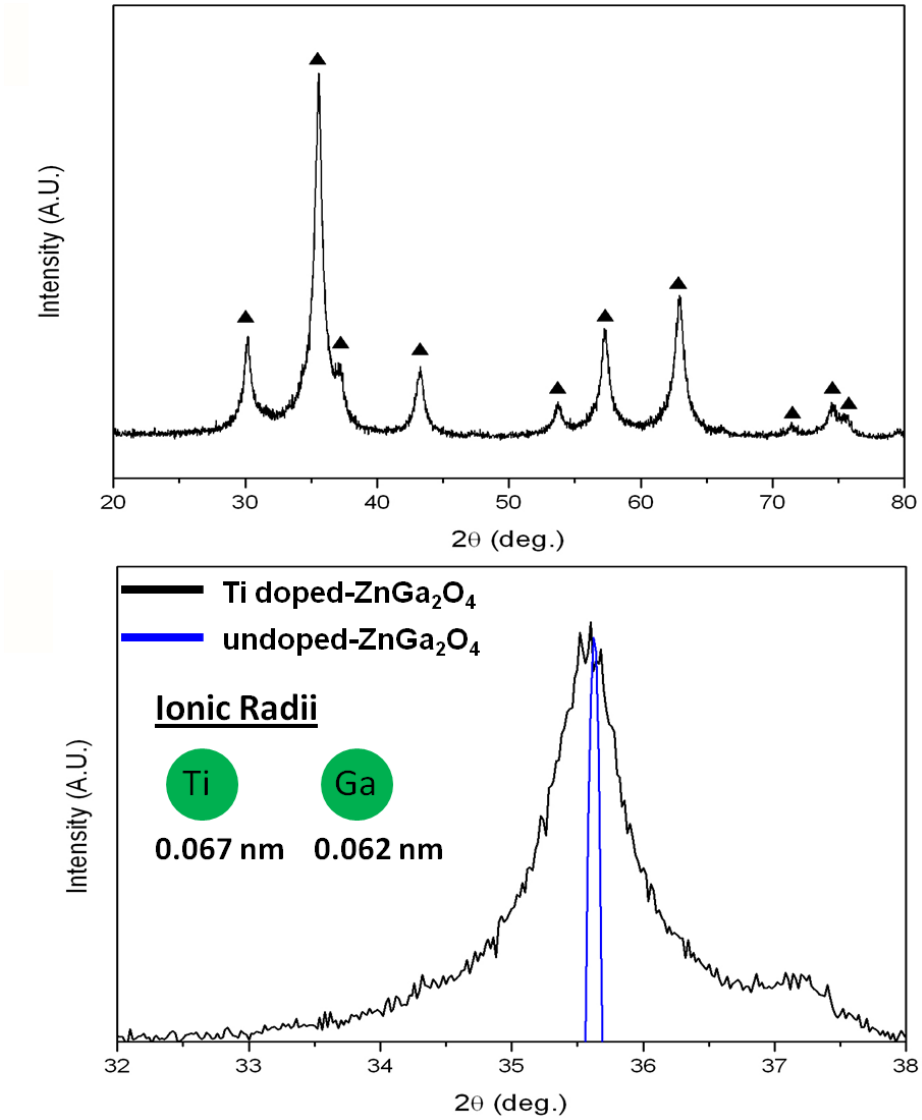

Figure 20. (top) Powder XRD patterns of Ti-doped $ZnGa_2O_4$. (bottom) Close comparison between Ti-doped and undoped $ZnGa_2O_4$.

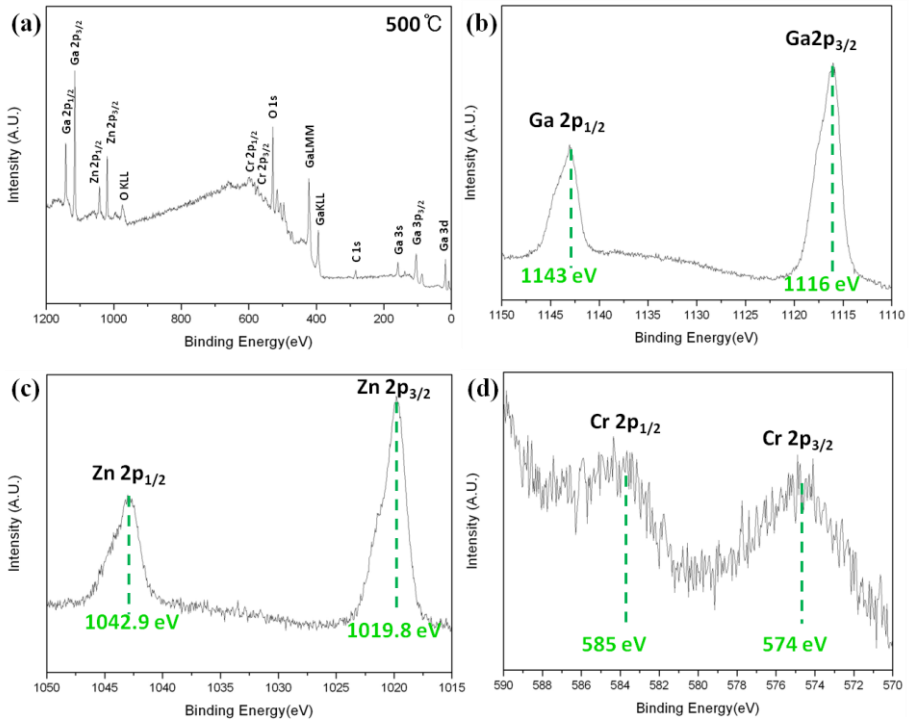

Figure 21. XPS spectra of Cr-doped $ZnGa_2O_4$: (a) wide scanning spectrum and the fine spectra of (b) Ga 2p, (c) Zn 2p, and (d) Cr 2p.

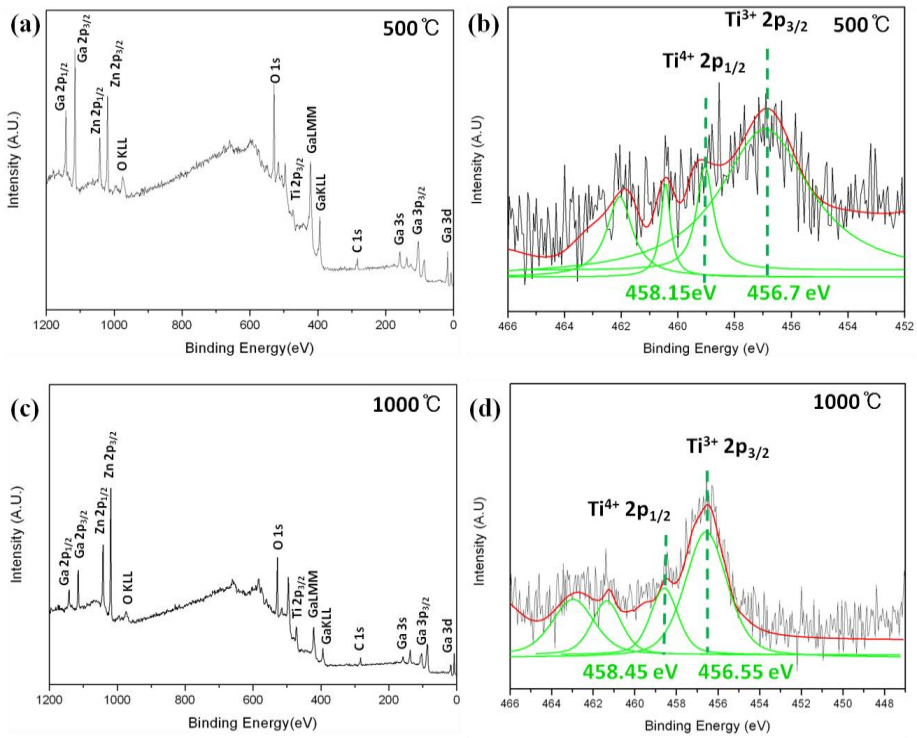

Figure 22. XPS spectra of Ti-doped $ZnGa_2O_4$: (a) wide scanning spectrum sample prepared at 500℃, (b) fine spectra of Ti 2p at 500℃, (c) wide scanning spectrum sample prepared at 1000℃, (d) fine spectra of Ti 2p at 1000℃.

3.2.3. Luminescence

In general, $ZnGa_2O_4$ with a band gap energy (Eg) of ~ 4.4 eV exhibits a strong blue emission due to the transition via a self-activation centre of Ga-O groups under excitation by ultraviolet light[21]. Moreover, its photoluminescence can be tuned via doping with a transition metal or rare-earth such as europium, terbium, manganese and chromium to emit red and green emission, achieving full RGB colour[39]. In this study, undoped, Cr^{3+}-doped and Ti^{3+}-doped $ZnGa_2O_4$ nanocrystalline powders were synthesized by liquid-phase combustion method, obtaining blue, red and bluish white-emitting $ZnGa_2O_4$ nanocrystal phosphors were discussed.

3.2.3.1.Photoluminescence of undoped $ZnGa_2O_4$

The Figure 23(a) shows the room-temperature PL emission spectra of nanosized $ZnGa_2O_4$ synthesized with metal nitrate and urea at different temperatures. In general, bulk $ZnGa_2O_4$ is reported to exhibit characteristic blue emission at about 430 nm originating from the self-activation centre of host material under excitation by UV light. However, $ZnGa_2O_4$ nanophosphor exhibit PL emission spectra peaks at 420, 470, 480, 490 nm when excited at 280 nm. The liquid-phase combustion have a much smaller particle size than those of conventional solid state reaction methods where introduction of quantum effect may play an important role[20]. Hence, synthesized nano $ZnGa_2O_4$ may lead to splitting of electronic energy levels of Ga^{3+} in the octahedral site of Ga-O, resulting splits in peaks observed at blue wavelength regions. Additionally, wavelength at about 550 nm is observed, which is generally obtained only by doping $ZnGa_2O_4$ with Mn^{2+}. Only few reports describe this emission which correspond to the transition between the photo-excited holes and singly-ionized oxygen vacancies[40]. It is also reported that

synthesis by organic containing precursor along with the use of combustion method generally leads to oxygen vacancies (V_O^*) originating the 680 nm emission peak[40]. Considering above statements, deconvolution of peaks were shown in Figure 23(b).

Additionally, first-principle approach, Discrete Variational Xα (DV-Xα) was used to estimate the emission mechanism, where the band gap of $ZnGa_2O_4$ was found to be about 5 eV (Appendix 2) which agrees very well to the referenced values[10,11]. However, for more detailed calculated result, further work on oxygen vacancy must be included for more detailed emission mechanism.

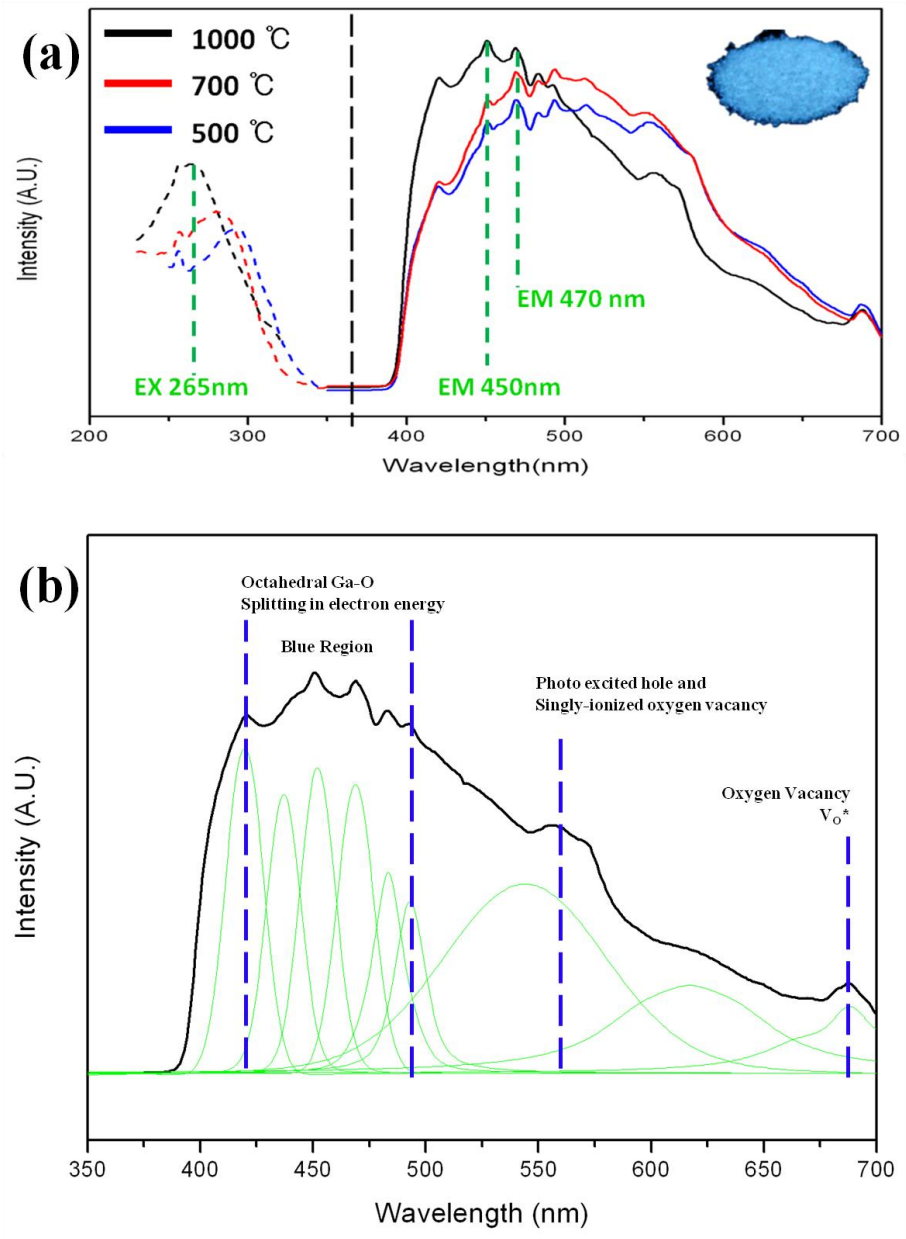

Figure 23. (a) Room-temperature PL emission spectra of nanosized $ZnGa_2O_4$ prepared at 500 (blue), 700 (red) and 1000℃ (black) excited at 265 nm.

(b) Deconvoluted graph of $ZnGa_2O_4$ synthesized at 1000℃-1h.

The PLE spectra of chromium-doped $ZnGa_2O_4$ and titanium-doped $ZnGa_2O_4$ are depicted in Figure 24. Both Cr-doped and Ti-doped were prepared at 500℃-1h. However, additional $ZnGa_2O_4:Ti^{3+}$ was prepared at 1000℃-1h reduce any confusion of emission raised from the organic molecules in titanium oxy-acetyl acetonate.

In Figure 24(a), Chromium doped-$ZnGa_2O_4$ shows high intensity at about 690 and 710 nm. The Cr^{3+} ions in $ZnGa_2O_4$ phosphor are generally well known for substitution in octahedral sites of Ga^{3+} ions to minimize charge and size variation. There are many reports that assign the excitation at 290 nm to the charge transfer of CrO^{6+}, $^4A_2$-$^4T_1$ transition of Cr^{3+} and the emission band of 700 nm is attributed to ^2E – $^4A_2$ transition of Cr^{3+} in octahedral sites[41,42]. Furthermore, the blue emission ranges between 400 to 600 nm are almost suppressed by Cr^{3+} showing red emission only.

The bluish white emission colour was observed with both $ZnGa_2O_4:Ti^{3+}$ synthesized at 500 and 1000℃ for 1h as seen in Figure 24(b). This bluish white emission is possibly due to the summation of different emission peaks involving three primary colour, depicted in Figure 24(b). Deconvolution peaks of $ZnGa_2O_4:Ti^{3+}$ prepared at 1000℃-1h is illustrated in Figure 25 showing all blue(B), green(YG) and red(R) region of visible wavelength. The emission intensity has dramatically decreased with the sample prepared at 500℃-1h possibly because nanosized particles consist of defect states that were lost by non-radiative emission.

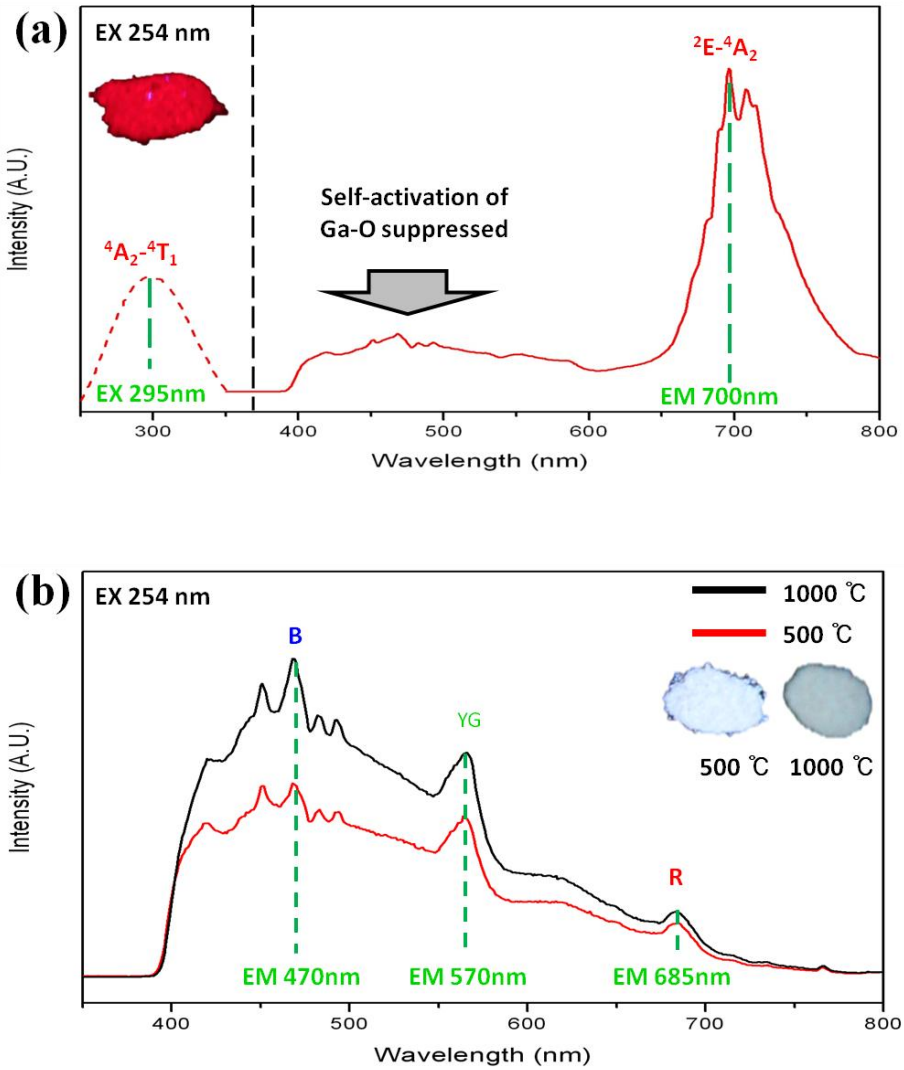

Figure 24. (a) PLE spectra of Cr-doped $ZnGa_2O_4$ excited at 295 nm and powder excited under UV-LEDs. (b) PLE spectra of Ti-doped $ZnGa_2O_4$ of sample prepared at 500(red) and 1000℃(black).

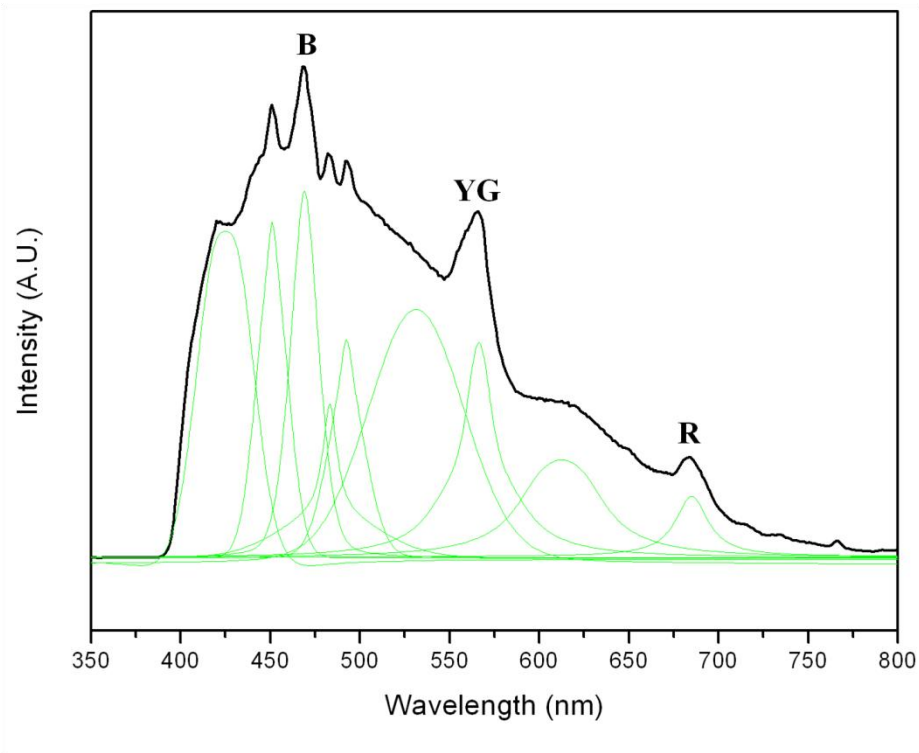

Figure 25. Deconvolution of PL of $ZnGa_2O_4:Ti^{3+}$ synthesized at 1000℃-1h, where B, YG, and R express red, yellow green and red region of visible wavelength.

3.2.4. Physical Properties of undoped – $ZnGa_2O_4$

Using the XRD result from Figure 17(a), the lattice parameter of each samples were estimated using the Bragg's law and illustrated in Figure 26.

$$d_{hkl} = \frac{a}{(h^2 + k^2 + l^2)^{\frac{1}{2}}}$$

The lattice parameter derived from XRD patterns varied with the growth temperature, generally increase in tendency from 8.33 to 8.36Å agreeing with reported values[43,44]. The result shows that lattice parameter of samples heat-treated at 500℃-1h has the lattice constant of about 8.34Å, on the other hand, the lattice parameter of samples prepared at higher temperature exceed the published values from ICSD data, 8.334Å. This phenomenon may be caused by difference in preparation technique and heating schedules of the spinel. She-Huang Wu et al[44] reported that production of $ZnGa_2O_4$ using citric sol-gel method, the decomposition of organic materials proceeded at 300 and 600℃. Although different organic containing materials were used, the decomposition temperature is believed to be in the similar range.

Hence, the abrupt augmentation in lattice parameter between 500 to 700℃ can be explained by the oxidation of oxygen-deficient powder. Since the organic residues were completely or almost decomposed at temperature higher than 500℃ as well as the improvement of crystallinity observed in Figure 17(a), rapid incorporation of oxygen may have occurred, causing distortion of oxygen ions within the spinel structure. On the other hand, the slight decrease in lattice parameter at 1000℃ is possibly due to oxygen loss from stabilizing the spinel structure of $ZnGa_2O_4$. The decrease in oxygen

contents can also be observed using the oxygen analysis technique illustrated in Table 5, showing lower weight % of oxygen in comparison to the bulk $ZnGa_2O_4$ synthesized by conventional solid state reaction method.

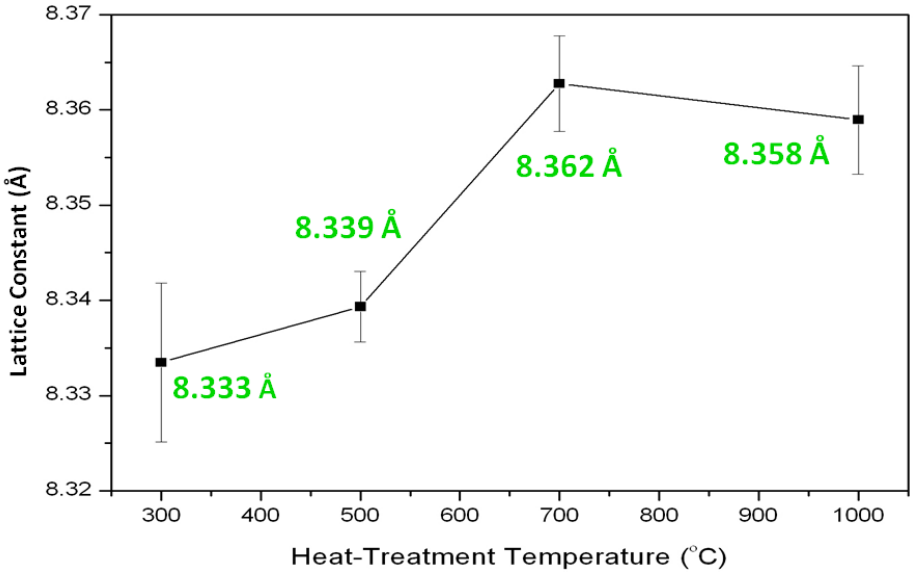

Figure 26. The variation of spinel lattice constant of 1h heat-treated stoichiometrically balanced $ZnGa_2O_4$ with different heat-treating temperature.

$ZnGa_2O_4$			
Synthesized Temperature (℃)	Bulk Oxygen(wt.%)	Nano Oxygen(wt.%)	Theoretical Oxygen(wt.%)
300	-	10.5	14.7
500	-	11.1	
700	-	11.9	
1000	13.8	10.9	

Table 5. Oxygen analysis of $ZnGa_2O_4$ synthesized at 300, 500, 700 and 1000℃-1h.

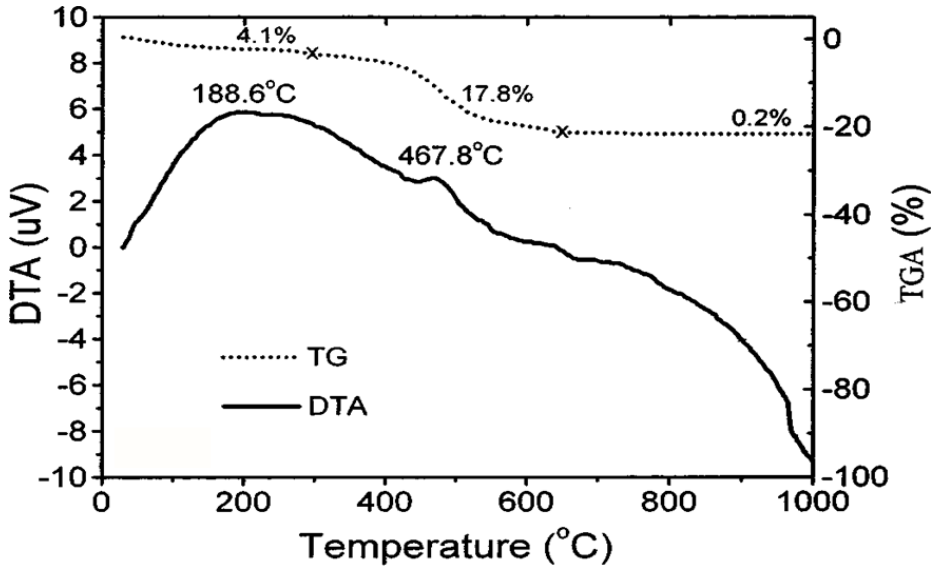

Figure 27. The DTA/TGA for the stoichiometric dried gel heated at 180℃ for 20h[44].

Furthermore, the average crystallite size (D) of each samples were estimated and represented in Figure 28 using the Scherrer equation and the diffraction patterns obtained from Figure 17(a), where λ is the X-ray wavelength (1.5405620Å), β is the ZnGa2O4 diffraction of (220), (311), (222), (400), (422), (511), and (440) peaks, and θ is the diffraction angle.

$$D = \frac{0.9\lambda}{\beta \cos\theta}$$

The average crystallite size estimated from XRD patterns varied with the synthesized temperature, generally showing increase in tendency. The average grain size of $ZnGa_2O_4$ differed with synthesis temperature, showing in the nano sized range (<100nm). The average crystallite size of $ZnGa_2O_4$ heat-treated at 300℃-1h was estimated about 5 nm and additionally varied with heat-treating temperatures. The largest crystallite size was obtained from 1000℃-1h estimated about 85 nm. For the comparison, bulk $ZnGa_2O_4$ was synthesized using ZnO and Ga_2O_3 at 1 to 1 ratio through conventional solid state reaction method depicted in Figure 11. Specifically, bulk $ZnGa_2O_4$ should be heat-treated above 1000℃ for several hours, but for convenience, synthetic schedule was chosen as 1000℃ for 4h in ambient atmosphere. Nevertheless, major diffraction peaks were well indexed with $ZnGa_2O_4$ and grain size estimation using the Scherrer method exceeded 100nm, which is beyond the definition of nanomaterials (European commission on 18th of October 2011). Furthermore, the secondary phase such as Ga_2O_3 was observed. Hence, the redox reaction by liquid-phase combustion method can be practically considered for the use of fabricating nano sized spinel for more pure spinel phase.

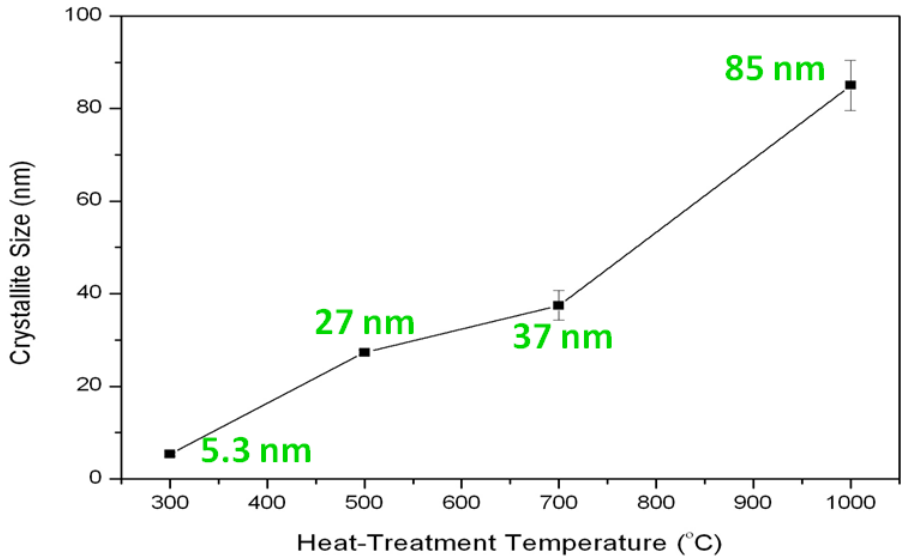

Figure 28. The Crystallite size of $ZnGa_2O_4$ heat-treated at different temperature for 1h.

3.2.5. Morphology

The high resolution transmission electron microscopy (HRTEM) analysis can provide more detailed structural information about $ZnGa_2O_4$ spinel. Figure 29 illustrate HRTEM images and XRD patterns of $ZnGa_2O_4$ synthesized at 300℃ for 1h in ambient atmosphere. The HRTEM image along with the electron diffraction patterns further confirms the formation of $ZnGa_2O_4$ that consists of single-crystal cubic spinel structure. Moreover, (111), (311), (220) planes are confirmed using electron diffraction patterns matching the published value from JCPDS entry #00-038-1240. However, agglomerations of particles are observed within the image. The combustion method generally involves ignition between metal nitrate and fuel, urea in our case. This allows highly exothermic reaction to proceed at lower temperature within a short time but generally owing to unavoidable agglomeration[27]. Nevertheless, the size of the spherically shaped particles was about 5nm smallest, which is consistent to the size derived from Scherrer method in previous result. In Figure 17, the crystallinity improved with increasing temperature suggesting the grain growth. Figure 30(a) illustrates the Field Emission Scanning Electron Microscopy (FE-SEM) image of ZnG_2O_4 prepared at 1000℃-1h. Again, highly agglomerated particles can be observed as well as increased in particle size. Figure 30(b) illustrates the size distribution of the $ZnGa_2O_4$ synthesized at 1000℃-1h. The average size was determined in between 70 to 80nm which is also consistent to the estimation. Additionally, clean surfaces of the particles were observed, suggesting the reason for its high intensity of luminescence property.

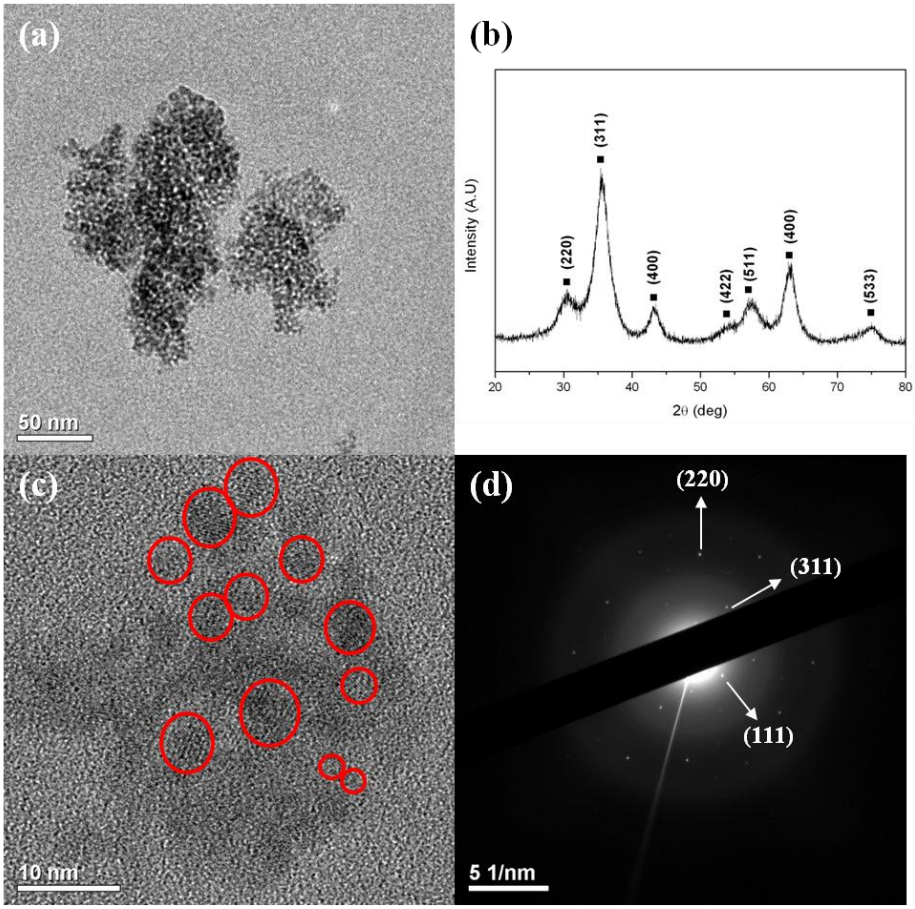

Figure 29. HRTEM images(a and c), powder XRD patterns and electron diffraction pattern of $ZnGa_2O_4$ synthesized at 300℃ for 1h.

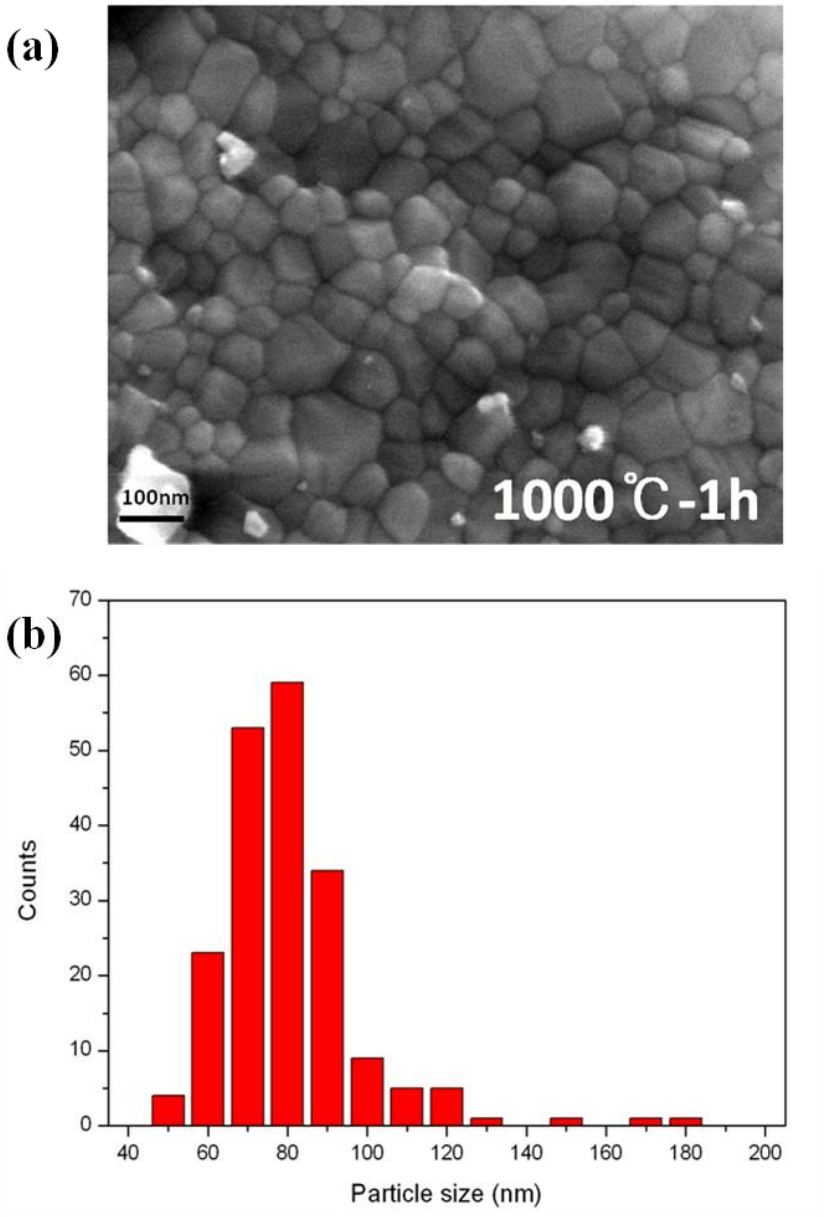

Figure 30. (a) FE-SEM image of $ZnGa_2O_4$ synthesized at 1000℃-1h and (b) its size distribution.

3.3. Effect of Organic impurity on $ZnGa_2O_4$

Research regarding organic-inorganic hybrid materials or organic containing inorganic materials have been highly investigated for the past few years due to its remarkable novel properties that could possibly be applied in conventional industry[45]. The co-occurrence of materials with multifunctional properties can be exploited with liquid-phase derived organic containing inorganic phosphor. Optical and electronic, thermal and chemical stability as well as biocompatibility are some of the characteristic features that will offer excellent prospects for material designers for specifically targeted applications, thus opening a new class of materials science and related technologies. In the aspect of the optical materials, full-colour phosphors may be achieved by controlling the size and organic reagent such as surfactant and capping agents. In this study, we have investigated the possibility of synthesizing organic-inorganic hybrid nanomaterials and its properties are discussed.

3.3.1. Luminescence

The Figure 31 shows the room-temperature PL emission spectra of nanosized $ZnGa_2O_4$ prepared with non-stoichiometrically balanced mixture system as ascribed in experimental procedure. A distinct difference in PL emission measurements are observed compared to the previous stoichiometrically balanced system seen in Figure 23. The spectrum shows a broad-band emission extending from 400 to 700 nm with a peak at 530 nm emitting yellow emission. After post heat-treatment at 1000℃ for 1h, the intrinsic blue emission returns, suggesting the degradation of organic materials. Ya-Ching. Yang et al[46] has reported an organic-inorganic hybrid gallium that emits intrinsic yellow light phosphor in a hybrid framework. However, yellow light emitting properties that containing gallium has not been reported much as far as we know.

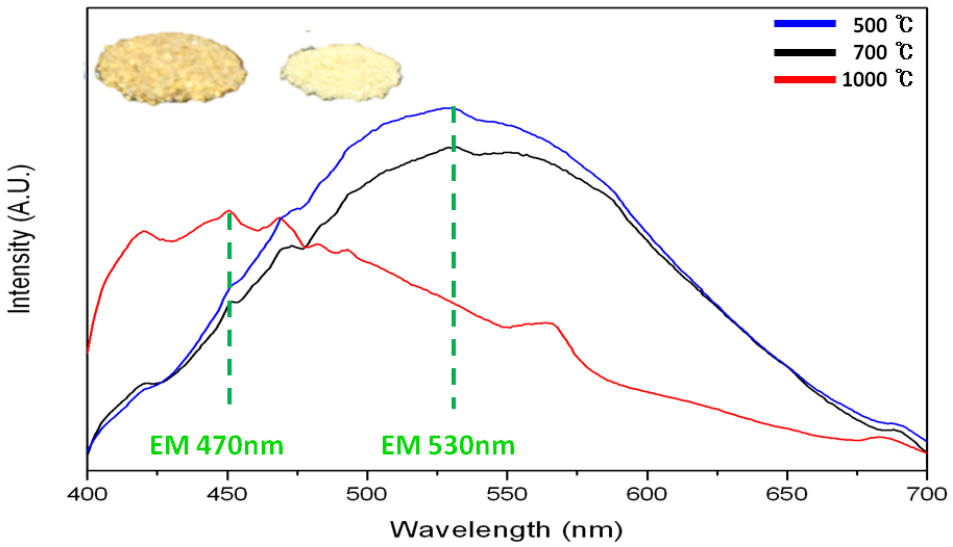

Figure 31. Room-temperature PL emission spectrum of the organic containing-$ZnGa_2O_4$ heat-treated at 500(blue), 700(black) and 1000℃(red).

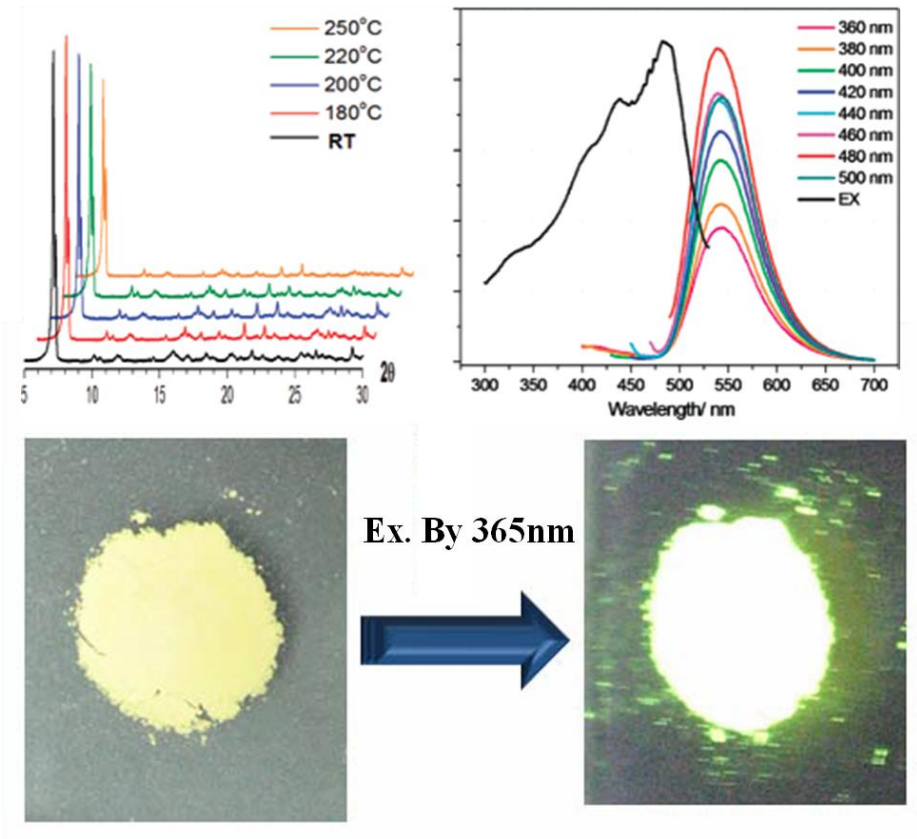

Figure 32. PXRD patterns measured at different temperatures (top left) and excitation and emission spectra of NTHU-6 (top right). Luminescence photos excited under 365 nm UV light[46].

3.3.2. Material Characterization of organic containing $ZnGa_2O_4$

Figure 33 illustrates the powder XRD patterns of $ZnGa_2O_4$ prepared by non-stoichiometrically balanced system heat-treated at 300, 500, 700, 1000 ℃ for 1h using zinc acetate dihydrate, $Zn(CH_3OO)_2{\cdot}2H_2O$, and $Ga(NO_3)_3{\cdot}xH_2O$ with addition of urea. According to S.R. Jain et al[32], $Zn(CH_3OO)_2{\cdot}2H_2O$ is also a reducing agent like urea. Hence, reduction of NO_x is less likely to occur and excess organic residues may remain within the system. The powder XRD patterns of all samples are in good agreement with JCPDS entry #00-038-1240, indicating a single phase $ZnGa_2O_4$ spinel structure.

Fourier Transform Infrared Spectroscopy (FT-IR) is one of the simplest and quickest analyzing techniques to determine the existence of organic through bond vibrations. Figure 34 illustrates the FT-IR spectra of organic containing-$ZnGa_2O_4$ hybrid material prepared at 500℃ for 1h, denoted AN(500), and 1000℃ for 1h, denoted AN(1000). The sample AN(500) shows vibrational bands at 580 and 640 cm^{-1} which originated from Zn-O-Ga and Ga-O. The broad vibration modes at around 450 to 530 cm^{-1} are assigned to Zn-O and 460 to 500 cm^{-1} are due to O-Ga-O bending mode[47]. The broad bands at 3400 and a peak at 1630 cm^{-1} correlated to H-O-H vibration modes of chemi-absorbed water molecules and vibration due to bending. Furthermore, the bands at 2963 and 3033 cm^{-1} may correspond to the C-H vibration from metal acetate, and the bands at 1550 and 1480 cm^{-1} are reported for a typical C=O and C-O vibrations when carbonyl groups coordinate with metal atoms in a bridging manner[48]. However, the 1550 cm^{-1} may also be ascribed to a C=N vibration. Also, two peaks at 2050 and 2200 cm^{-1} may corresponds to C≡C or C≡N but more evidence will be required.

Above all, possibility of a ‘shell’ of organic molecules may be attached to the surface of the nanoparticles. The FT-IR of AN(1000), blue line, shows a distinct decrease in intensity with removal of two peaks at 2200 and 2050 cm^{-1}. In previous PLE emission from Figure 34 (bottom), broad yellow emission has returned to its original emission colour after heat-treatment at 1000℃-1h, AN(PH1000). This suggest how ‘shell’ of organic molecules are strongly attached to the inorganic $ZnGa_2O_4$ spinel, nevertheless, high temperature heating will eventually decompose the organic ‘shell’.

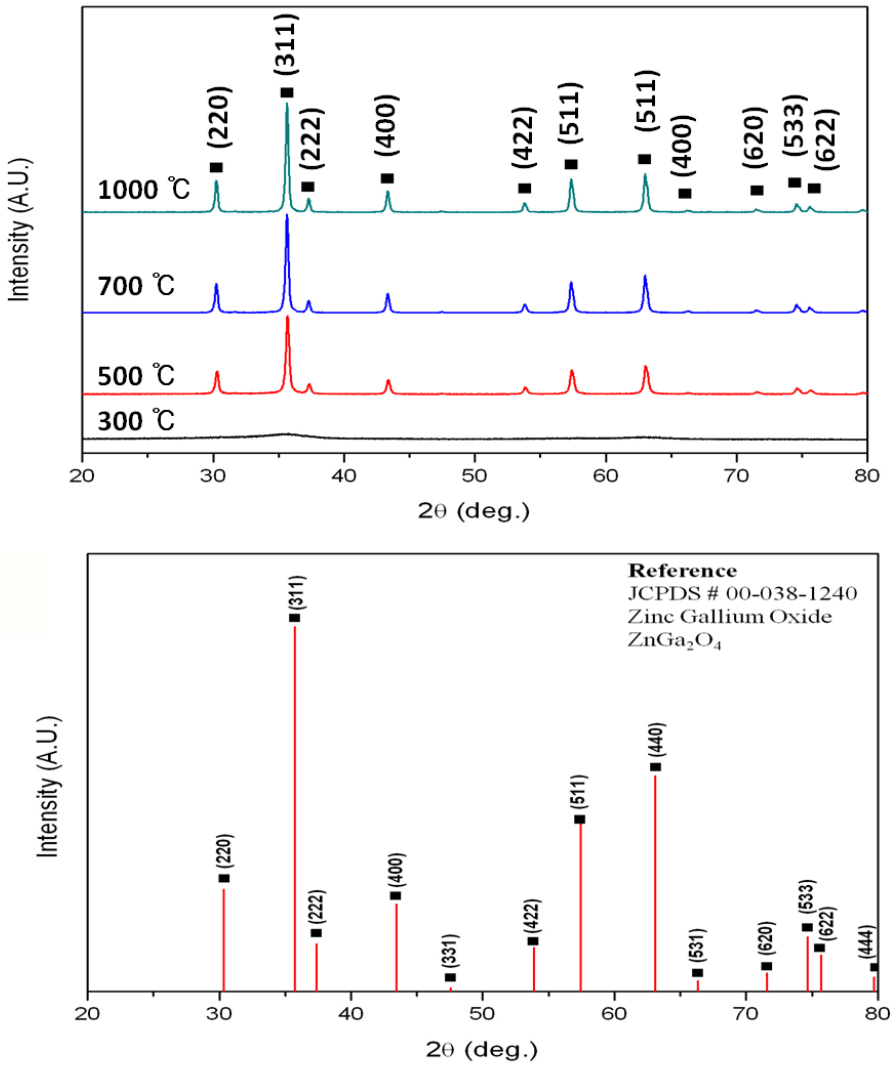

Figure 33. (top)Powder XRD patterns of organic containing $ZnGa_2O_4$ at (a) 300, (b) 500, (c) 700, and (d) 1000℃-1h. (bottom) XRD patterns of $ZnGa_2O_4$ reference from JCPDS #00-038-1240.

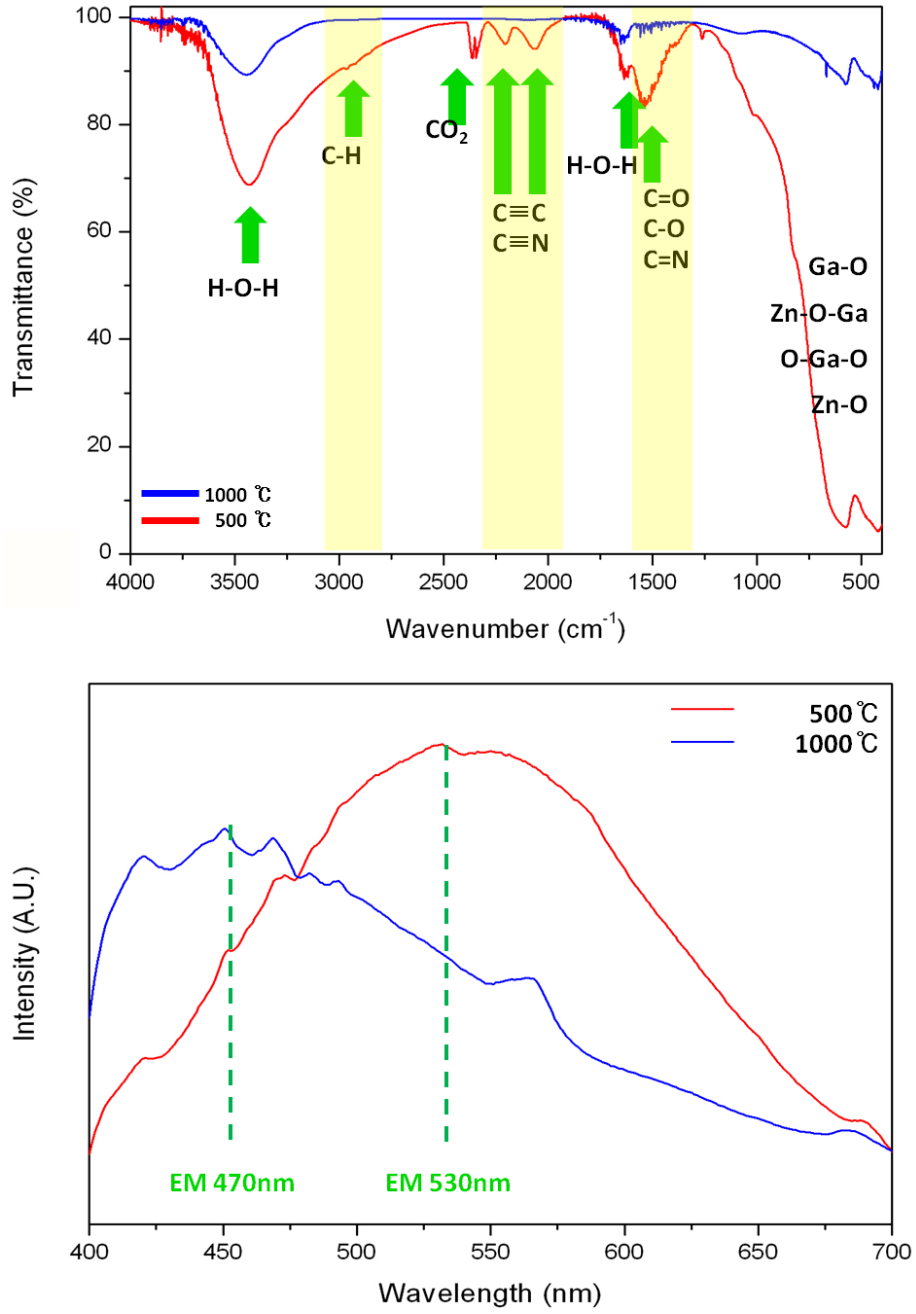

Figure 34. (top) FT-IR spectra of AN(500) (red) and AN(1000) (blue). (bottom) PLE spectra of AN(500) (red) and AN(1000) blue.

Having much broader powder XRD patterns than stoichiometrically balanced system, HRTEM and FESEM were used to further analyze the produced sample's size and its morphology. Figure 35 illustrates the HRTEM image non-stoichiometrically balanced $ZnGa_2O_4$ prepared at 300℃ for 1h. Figure 35(a) shows more variable size distribution compare to the stoichiometrically balanced system, where the average size is between 2 to 10 nm. Figure 35(c) shows well developed lattice fringes which on the one hand confirm the high crystallinity of the sample even though Figure 35(b) shows broad XRD patterns. Additionally, the electron diffraction depicted in Figure 35(d) further confirms the existence of $ZnGa_2O_4$.

The FE-SEM image of $ZnGa_2O_4$ prepared with non-stoichiometrically balanced system heat-treated at 1000℃ for 1h is depicted in Figure 36. The average particle size was about 55 nm, which is in fact 20 nm smaller than the previous stoichiometrically system. The non-stoichiometrically balanced system is expected with excess organic residues, which may surround the inorganic $ZnGa_2O_4$. Since the grain growth will be hindered by surrounding organic 'shell', the smaller average particle size in Figure 36 can be explained.

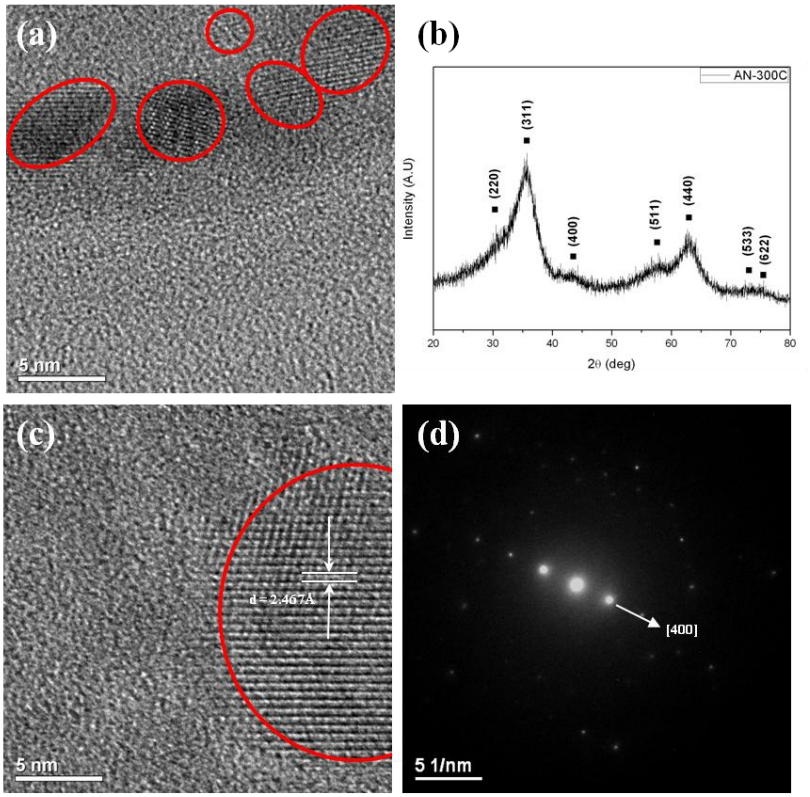

Figure 35. (a) and (c) HRTEM of organic containing $ZnGa_2O_4$ synthesized at 300℃-1h, (b) Powder XRD patterns and (d) Electron diffraction patterns.

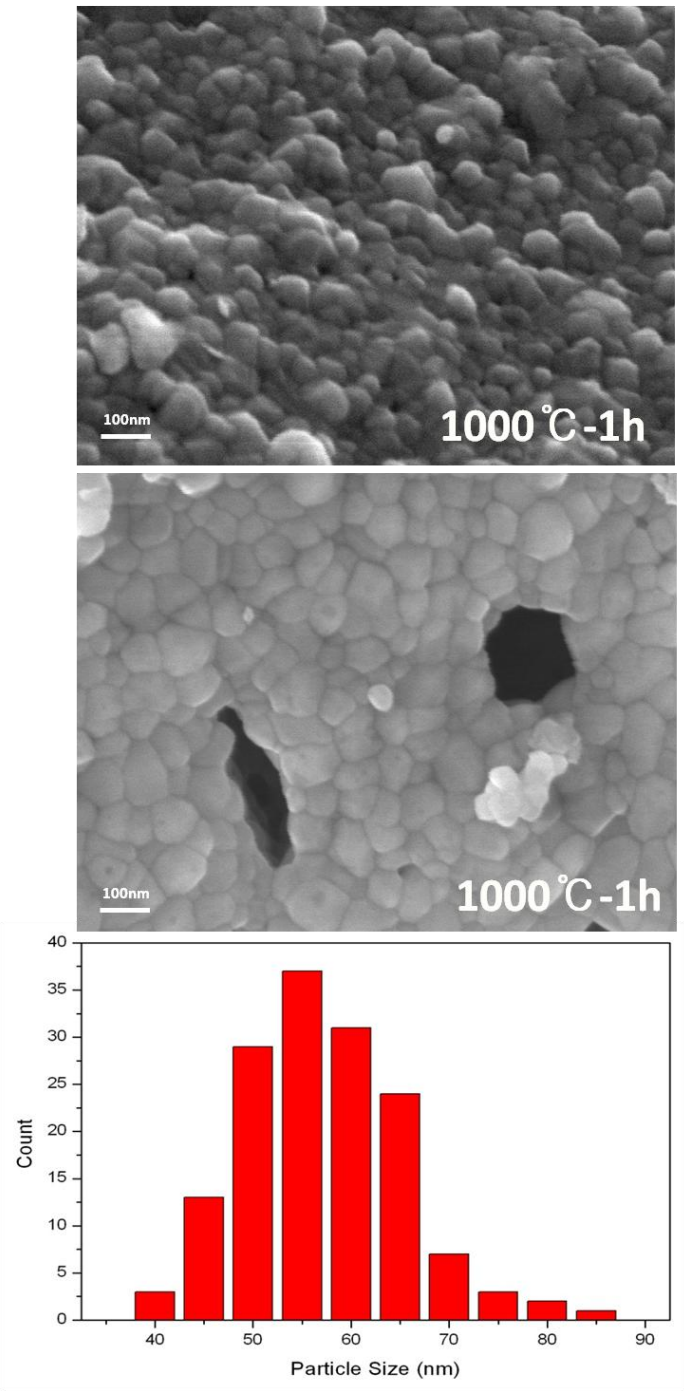

Figure 36. (top and middle) FE-SEM image of $ZnGa_2O_4$ prepared by non-stoichiometrically balanced system. (bottom) Size distribution.

Chapter 4. Conclusions

In summary, we have developed a new route to synthesize luminescent undoped and 0.02 mol. fraction% of Cr, Ti doped $ZnGa_2O_4$ nanoparticles through a simple liquid-phase combustion method with addition of urea, which has successfully synthesized $ZnGa_2O_4$ nanocrystals by varying the process parameters such as temperature and doping elements. XRD these nanoparticles have spinel structure and the smallest average particle size obtained from 300℃-1h heat-treatment was estimated at 5 nm, which was confirmed by HRTEM.

The UV excitation at 290 nm shows blue PL emission between 420 to 490 nm appeared to be due to the quantum confinement effect, splitting of electronic energy levels of Ga^{3+}. PL emission at 550 nm was observed due to the transition between the photo-excited holes and singly-ionized oxygen vacancies. Furthermore, the 680 nm emission peak was originated from oxygen vacancy, which often appears during the use of organic precursors along with combustion method. However, no other secondary phases were observed through XRD and XPS other than small amount of carbon impurity.

The red PL emissions from the $^2E - {}^4A_2$ transition of Cr^{3+} ions are observed under an excitation of 290 nm. The XPS spectra reveal successful substitution of chromium into gallium octahedral site and no other secondary phases have been detected. The bluish white PL emission was also observed from Ti doped-$ZnGa_2O_4$ with same excitation, where XPS spectrum shows the existence of both Ti^{3+} and Ti^{4+} oxidation state at the surface. However, the majority of trivalent Ti^{3+} exists at the surface suggesting the occupation in Ga^{3+} octahedral position.

A broad yellow PL emission at 530 nm was obtained from organic containing inorganic phosphor material, where non-stoichiometrically balanced system was intentionally introduced. The average particle size was confirmed in between 2 to 10 nm when synthesized at 300℃-1h. The small particle size seems to be attributed due to the ‘shell’ of these organic molecules surrounding the $ZnGa_2O_4$, hindering the grain growth. This yellow PL emission sample could be the potential yellow phosphor but it also has potential use in the field of biotechnology with careful analysis and modification of organic functional groups.

Appendix

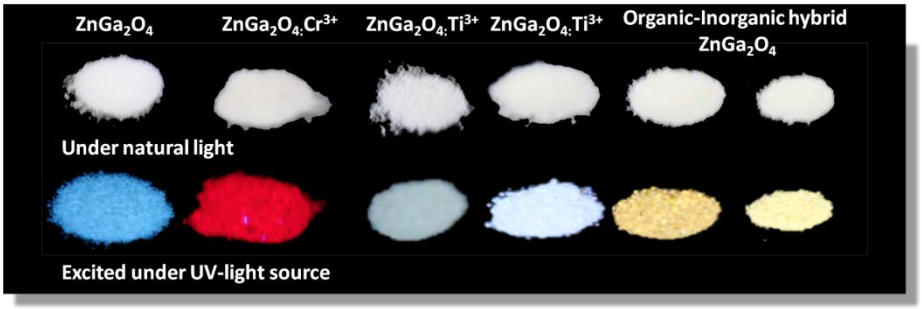

Appendix 1. Luminescence photos of doped, undoped, and organic containing $ZnGa_2O_4$ synthesized through liquid phase combustion methods.

The bandgap of $ZnGa_2O_4$ was calculated using Discrete variational Xα (DV-Xα). For this method, $[Zn_6Ga_{19}O_{88}]^{-7}$ cluster was applied which is illustrated in Appendix 2(a). The energy diagram reveals that the bandgap of $ZnGa_2O_4$ is about 5 eV which is similar to some reported experimental values[10,11].

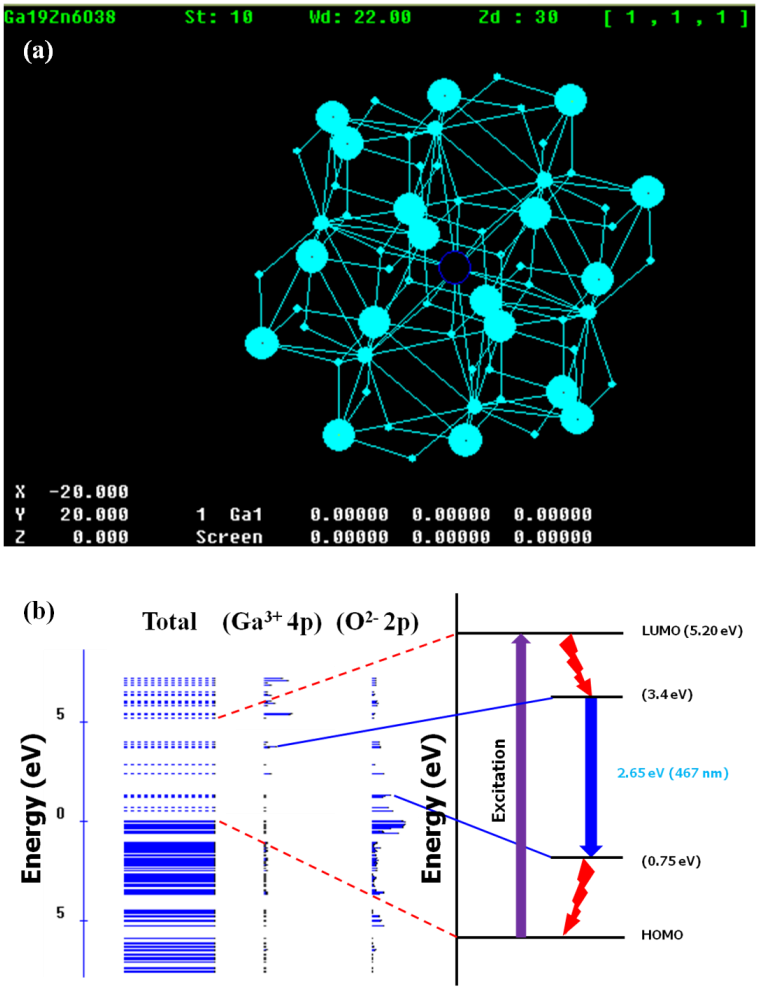

Appendix 2. (a) $[Zn_6Ga_{10}O_{38}]^{-7}$ cluster used for calculation. (b) Band gap of $ZnGa_2O_4$ calculated by DV-Xα.

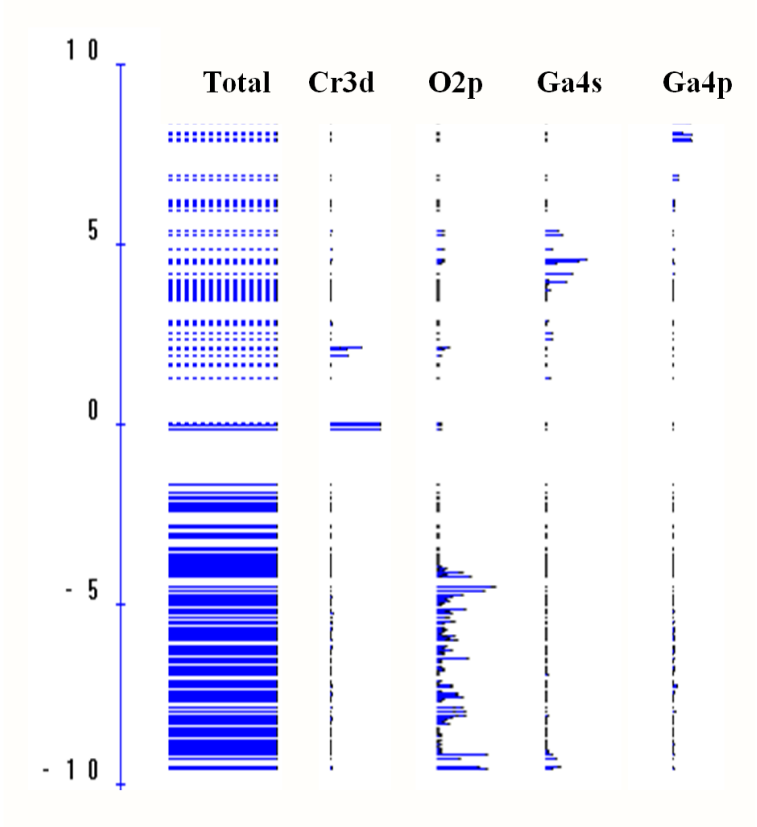

Appendix 3. Calculated energy level of $ZnGa_2O_4:Cr^{3+}$ from DV-Xα.

Although, calculated result shows the energy level of $ZnGa_2O_4:Cr^{3+}$, this data do not include any vacancies. Further work will be required for more precise calculation by addition of oxygen vacancies.

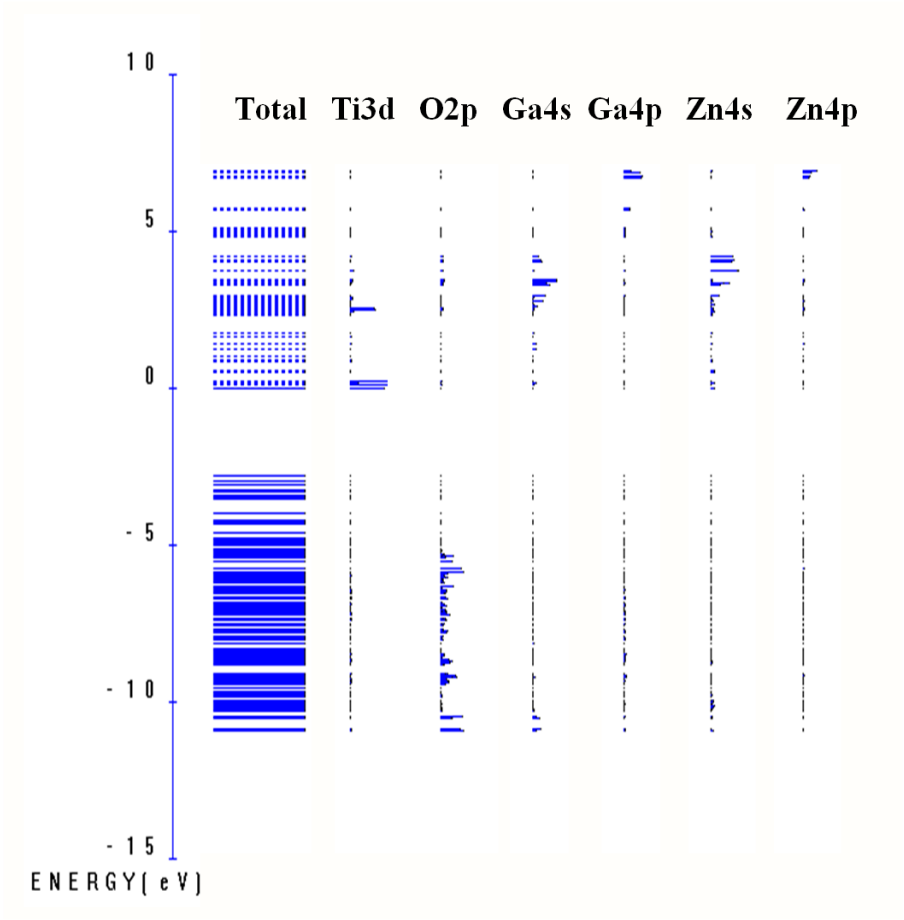

Appendix 4. Calculated energy level of $ZnGa_2O_4:Ti^{3+}$ from DV-Xα.

Similarly, the produced energy level is from pure $ZnGa_2O_4:Ti^{3+}$ meaning defects or oxygen vacancy have not been included during the calculation. The data may be referred for finding the optical band gap but for more precise data, addition of defects such as oxygen vacancy is critical.

Reference

[1] K. N. Shinde, S. J. Dhoble, H. C. Swart, K. Park (2012) Phosphate Phosphors for Solid-State Lighting (Springer-Verlag).

[2] G. Blasse, B. C. Grabmaier (1994) Luminescent Materials (Springer-Verlag).

[3] J. Madigan, L. Chambers. (2011) National Aeronautics and Space Administration. http://science-edu.larc.nasa.gov/EDDOCS/Wavelengths_for_Colors.html [Accessed 16th May 2013].

[4] J. Reichman, (2010) Handbook of Optical Filters for Fluorescence Microscopy (Chroma Technology, Brattleboro).

[5] Geffroy, B., P. le Roy and C. Prat (2006). "Organic light-emitting diode (OLED) technology: materials, devices and display technologies." Polymer International 55(6): 572-582.

[6] Lin, C. C. and R.-S. Liu (2011). "Advances in Phosphors for Light-emitting Diodes." The Journal of Physical Chemistry Letters 2(11): 1268-1277.

[7] R. Halliday(ed.) (2010) Key Benefits of Next-Gen UV LED Technology Lumex, Inc.

[8] Itoh, S., H. Toki, Y. Sato, K. Morimoto and T. Kishino (1991). "THE ZNGA2O4 PHOSPHOR FOR LOW-VOLTAGE BLUE CATHODOLUMINESCENCE." Journal of the Electrochemical Society 138(5): 1509-1512.

[9] Sickafus, K. E., J. M. Wills and N. W. Grimes (1999). "Structure of Spinel." Journal of the American Ceramic Society 82(12): 3279-3292.

[10] Phani, A. R., S. Santucci, S. Di Nardo, L. Lozzi, M. Passacantando, P. Picozzi and C. Cantalini (1998). "Preparation and characterization of bulk ZnGa2O4." Journal of Materials Science 33(15): 3969-3973.

[11] Shi, Q., J. Y. Zhang, C. Cai, L. Cong and T. M. Wang (2008). "Synthesis and photoluminescent properties of Eu3+-doped ZnGa2O4 nanophosphors." Materials Science and Engineering B-Advanced Functional Solid-State Materials 149(1): 82-86.

[12] Hsu, K. H., M. R. Yang and K. S. Chen (1998). "A study of ZnGa2O4 phosphor prepared by the solid method." Journal of Materials Science-Materials in Electronics 9(4): 283-288.

[13] Zou, L., X. Xiang, M. Wei, F. Li and D. G. Evans (2008). "Single-crystalline ZnGa2O4 spinet phosphor via a single-source inorganic precursor route." Inorganic Chemistry 47(4): 1361-1369.

[14] Takesada, M., T. Isobe, H. Takahashi and S. Itoh (2007). "Glycothermal synthesis of ZnGa2O4 : Mn2+ nanophosphor and change in its photoluminescence intensity by heat-treatment." Journal of the Electrochemical Society 154(4): J136-J140.

[15] Rack, P. D., J. J. Peterson, M. D. Potter and W. Park (2001). "Eu+3 and Cr+3 doping for red cathodoluminescence in ZnGa2O4." Journal of Materials Research 16(5): 1429-1433.

[16] Lim, J. H., B. N. Kim, Y. Kim, S. Kang, R. J. Xie, I. S. Chong, K. Morita, H. Yoshida and K. Hiraga (2013). "Non-rare earth white emission phosphor: Ti-doped MgAl2O4." Applied Physics Letters 102(3).

[17] Zhuang, Y. X., J. Ueda and S. Tanabe (2012). "Photochromism and white long-lasting persistent luminescence in Bi3+-doped ZnGa2O4 ceramics." Optical Materials Express 2(10): 1378-1383.

[18] Allix, M., S. Chenu, E. Véron, T. Poumeyrol, E. A. Kouadri-Boudjelthia, S. Alahraché, F. Porcher, D. Massiot and F. Fayon (2013). "Considerable Improvement of Long-Persistent Luminescence in Germanium and Tin Substituted ZnGa2O4." Chemistry of Materials 25(9): 1600-1606.

[19] Zhou, W., X. Yang, L. Huang, J. Wang, J. Tang and H. Liang (2012). "Synthesis of porous zinc gallate prisms composed of highly oriented

nanoparticles by an in situ conversion reaction." Chemistry 18(17): 5367-5373.

[20] Cao, M., I. Djerdj, M. Antonietti and M. Niederberger (2007). "Nonaqueous synthesis of colloidal ZnGa2O4 nanocrystals and their photolinninescence properties." Chemistry of Materials 19(24): 5830-5832.

[21] Byun, H. J., J. U. Kim and H. Yang (2009). "Blue, green, and red emission from undoped and doped ZnGa2O4 colloidal nanocrystals." Nanotechnology 20(49).

[22] Gu, Z. J., F. Liu, X. F. Li, J. Howe, J. Xu, Y. L. Zhao and Z. W. Pan (2010). "Red, Green, and Blue Luminescence from ZnGa2O4 Nanowire Arrays." Journal of Physical Chemistry Letters 1(1): 354-357.

[23] Pileni, M. P. (2003). "The role of soft colloidal templates in controlling the size and shape of inorganic nanocrystals." Nature Materials 2(3): 145-150.

[24] Zhong, M., Y. B. Li, I. Yamada and J. J. Delaunay (2012). "ZnO-ZnGa2O4 core-shell nanowire array for stable photoelectrochemical water splitting." Nanoscale 4(5): 1509-1514.

[25] Farvid, S. S., T. Wang and P. V. Radovanovic (2011). "Colloidal Gallium Indium Oxide Nanocrystals: A Multifunctional Light-Emitting Phosphor Broadly Tunable by Alloy Composition." Journal of the American Chemical Society 133(17): 6711-6719.

[26] Jun, Y. W., J. S. Choi and J. Cheon (2006). "Shape control of semiconductor and metal oxide nanocrystals through nonhydrolytic colloidal routes." Angewandte Chemie-International Edition 45(21): 3414-3439.

[27] Han, J. K., J. I. Choi, A. Piquette, M. Hannah, M. Anc, M. Galvez, J. B. Talbot and J. McKittrick (2012). "Phosphor Development and Integration for Near-UV LED Solid State Lighting." ECS Journal of Solid State

Science and Technology 2(2): R3138-R3147.

[28] Kakihana, M. (1996). ""Sol-Gel" preparation of high temperature superconducting oxides." Journal of Sol-Gel Science and Technology 6(1): 7-55.

[29] Park, J. K., M. A. Lim, C. H. Kim, H. D. Park, J. T. Park and S. Y. Choi (2003). "White light-emitting diodes of GaN-based Sr2SiO4 : Eu and the luminescent properties." Applied Physics Letters 82(5): 683-685.

[30] Zhang, Q. Y. and X. Y. Huang (2010). "Recent progress in quantum cutting phosphors." Progress in Materials Science 55(5): 353-427.

[31] Han, J. K., M. E. Hannah, A. Piquette, G. A. Hirata, J. B. Talbot, K. C. Mishra and J. McKittricka (2012). "Structure dependent luminescence characterization of green-yellow emitting Sr2SiO4:Eu2+ phosphors for near UV LEDs." Journal of Luminescence 132(1): 106-109.

[32] Jain, S. R., K. C. Adiga and V. R. P. Verneker (1981). "A NEW APPROACH TO THERMOCHEMICAL CALCULATIONS OF CONDENSED FUEL-OXIDIZER MIXTURES." Combustion and Flame 40(1): 71-79.

[33] Kim, Y. and S. Kong (2011). "Effect of particle size on photoluminescence emission intensity in ZnO." Acta Materialia 59(8): 3024-3031.

[34] Adachi, H., M. Tsukada and C. Satoko (1978). "DISCRETE VARIATIONAL X-ALPHA CLUSTER CALCULATIONS .1. APPLICATION TO METAL CLUSTERS." Journal of the Physical Society of Japan 45(3): 875-883.

[35] Slater, J. C. (1951). "A SIMPLIFICATION OF THE HARTREE-FOCK METHOD." Physical Review 81(3): 385-390.

[36] Ashrul Ishak, M. S. and M. N. Mohd. Jaafar (2011). "The Used of Aqueous Urea Solution in Reduction of Noxious Emissions in Bio Fuel Combustion System Using Selective Non-Catalytic Reduction." Modern

Applied Science 5(4).

[37] J. F. Moulder, W. F. Stick, P. E. Sobol and K. D. Bomben, Handbook of X-ray Photoelectron Spectroscopy, ed. J. Chanstain and R. C. King Jr., Physical Electronics, Inc., USA, 1992.

[38] Hashimoto, S. and A. Tanaka (2002). "Alteration of Ti 2p XPS spectrum for titanium oxide by low-energy Ar ion bombardment." Surface and Interface Analysis 34(1): 262-265.

[39] Zhitari, V. F., S. P. Muntean and V. I. Pavlenko (2009). "Photoluminescence of ZnGa2O4 doped with Mn, Yb, Sm, and Tb." Inorganic Materials 45(3): 278-280.

[40] Kim, J. S., H. I. Kang, W. N. Kim, J. I. Kim, J. C. Choi, H. L. Park, G. C. Kim, T. W. Kim, Y. H. Hwang, S. I. Mho, M. C. Jung and M. Han (2003). "Color variation of ZnGa2O4 phosphor by reduction-oxidation processes." Applied Physics Letters 82(13): 2029-2031.

[41] Kim, J. S., J. S. Kim and H. L. Park (2004). "Optical and structural properties of nanosized ZnGa2O4 : Cr3+ phosphor." Solid State Communications 131(12): 735-738.

[42] Bessiere, A., S. Jacquart, K. Priolkar, A. Lecointre, B. Viana and D. Gourier (2011). "ZnGa2O4:Cr3+: a new red long-lasting phosphor with high brightness." Optics Express 19(11): 10131-10137.

[43] Kim, J. S., H. L. Park, C. M. Chon, H. S. Moon and T. W. Kim (2004). "The origin of emission color of reduced and oxidized ZnGa2O4 phosphors." Solid State Communications 129(3): 163-167.

[44] Wu, S. H. and H. C. Cheng (2004). "Preparation and characterization of nanosized ZnGa2O4 phosphors." Journal of the Electrochemical Society 151(7): H159-H163.

[45] Carlos, L. D., R. A. S. Ferreira, V. D. Bermudez, B. Julian-Lopez and P. Escribano (2011). "Progress on lanthanide-based organic-inorganic hybrid phosphors." Chemical Society Reviews 40(2): 536-549.

[46] Yang, Y. C. and S. L. Wang (2008). "Intrinsic yellow light phosphor: An organic-inorganic hybrid gallium oxalatophosphate with hexameric octahedral Ga-6(OH)(4)O-26 cluster." Journal of the American Chemical Society 130(4): 1146-+.

[47] Can, M. M., G. H. Jaffari, S. Aksoy, S. I. Shah and T. Firat (2013). "Synthesis and characterization of ZnGa2O4 particles prepared by solid state reaction." Journal of Alloys and Compounds 549: 303-307.

[48] Aneesh, P. M., K. M. Krishna and M. K. Jayaraj (2009). "Hydrothermal Synthesis and Characterization of Undoped and Eu-Doped ZnGa2O4 Nanoparticles." Journal of the Electrochemical Society 156(3): K33-K36.

국문 초록

이 문 균 (Mun Keun Lee)

재료공학부

대학원

서울대학교

Zinc Gallate ($ZnGa_2O_4$) 와 같이 넓은 Band Gap을 갖고 있는 산화물 반도체가 최근 많은 각광 받고 있는 이유는, 이것이 UV-emitter 형광체 모체로서 FED, thin-film electroluminescent 디스플레이 등을 포함한 다양한 분야에 높은 응용 가능성을 가지고 있기 때문이다. 산화물 기반의 $ZnGa_2O_4$ Spinel 구조를 갖는 형광체는 흥미로운 전기적, 기계적, 자성적, 광학적 특성 때문에 연구소재로서 관심 있게 연구되어 왔다. 또한 나노기술의 적용으로 보다 넓은 분야에 다양하게 응용이 가능하다.

현재까지 많은 합성방법들이 제안되었지만, 이 논문에서는, 본 실험실에서 개발된 액상연소법을 사용하여, $ZnGa_2O_4$을 금속-유기전구체와 유기연료 (urea) 간의 화학 양론적 균형을 이루는 완벽한 산화환원 반응을 통하여, 약 5nm의 크기를 갖는 나노 입자로 만들었다. 또한, 본 연구에서는, $ZnGa_2O_4$ 의 광학적 특성과 transition metal의 도핑 (chromium, titanium) 여부로 emission 의 특성 조절을 중점적으로 다루어 청색, 적색, 푸르스름한 백색의 형광특성을 달성하였다. Ga-O에서 발현된 청색 emission은 280nm 여기광 self-excitation으로부터 비롯되었다. 이러한 emission 특성은 photoluminescence spectra을 통하여 관찰하였고 이 값은 에너지

다이어그램 계산으로 설명할 수 있었다.

$ZnGa_2O_4$ 의 Band Gap 에너지는 제일 계산원리를 (DV-Xα) 통하여 약 5eV로 계산되었으며 이 값은 기존의 문헌값과도 일치한다. 물론, 좀 더 정확한 계산을 하기 위해서는 Oxygen Vacancy의 고려가 필요할 것으로 보인다. 또한, 희토류 족 원소의 첨가 없이, transition metal 도핑만으로 높은 강도의 적색 및 푸르스름한 백색 형광특성이 확인되었다.

추가적으로, 비-화학 양론적 산화환원 반응으로 유기적 결함이 $ZnGa_2O_4$ 형광체 내에 주는 광학적 효과를 조사하였다. 이 비-화학 양론적 산화환원반응을 통하여, $ZnGa_2O_4$ 형광체는 높은 강도의 황색 emission을 보였고, 1000℃ 이상의 열처리 시, 본래의 청색 emission 특성을 나타냄과 동시의 고온에서의 높은 열적 안정성을 보여주었다. 본 연구에서는 앞서 기술한 결과를 Organic-Bridging 와 유기적 결함의 관점에서 접근 하였다.

이 논문에서는, bulk 와 nano 크기의 도핑 되거나 혹은 도핑되지않은 $ZnGa_2O_4$ 의 광학적 특성의 이해와 함께 $ZnGa_2O_4$ 와 결합한 유기적 작용기의 효과를 실험적으로 관찰 하였고 이를 이론적으로 규명하고자 하였다.

핵심어: Phosphor, Photoluminescence, Luminescence, Organic Impurity, $ZnGa_2O_4$, Nanocrystals.

학 번: 2011-24049

Acknowledgement (in Korean)

감사의 글

2011 년 6 월, 서울대학교에 군복을 입은 상태로 면접실을 찾느라 고생했던 때가 엊그제 같은데 벌써 2 년이라는 시간이 흘러 제가 벌써 석사를 맞추고 감사의 글을 적으니 실감이 나지 않습니다. 처음에는 느리게만 흘러가던 시계 바늘이 졸업학기에는 너무도 빨리 지나가 마음이 무거워졌으나 이럴때마다 저에게 많은 힘을 실어주신 여러분들께 감사의 글로 저의 마음을 조금이나마 전달해드리고자 합니다.

먼저, 저의 지도 교수님이신 강신후 교수님께 감사의 말씀을 드립니다. 아직도 교수님과 처음으로 말씀을 나누었던 날이 생생합니다. 당시 군대에 있던 저를 반갑게 맞아주시며 한국 대학원 생활을 잘 알지 못하는 저에게 너무나도 다정하게 '아무걱정없이 군제대 잘 하고 오면 돼' 라는 말씀과 함께 CMC 라는 너무나도 좋은 연구실로 받아주셔서 그 당시 얼마나 기뻤는지 모르겠습니다. 석사과정동안 학문적 지도뿐 아니라, 성경공부로 저의 삶을 하나님께 한층 더 가깝게 다가갈수 있게 도와주신 점, 또한 아들처럼 아껴주시고 사랑해주신 교수님께 감사 드립니다. 또한, 늘 저희를 환하게 맞아주시던 강윤희 사모님께도 감사드립니다. 성경공부 시간에 사모님께서 해주시는 솔직하신 말씀들은 큰 도움이 된 것 같습니다. .

또한, 저의 석사 논문 심사를 맡아주신 홍성현 교수님과 남기태 교수님께도 감사의 말씀을 드립니다. 심사 때 제게 해주신 귀중한 조언들은 졸업 논문을 쓸 때 많은 도움이 되었고 논문심사 후 저에게 해주신 격려는 앞으로 저의 박사과정 동안에 너무나도 큰 힘이 될 것 같습니다. 감사드립니다.

석사 생활 중 저에게 있어 가장 큰 선물은 인연인 것 같습니다. CMC 를 통한 인연으로 지난 2 년간 만난 멤버, 선·후배님들께 감사의 말씀을 적으려고 합니다. 들어와서 몇 개월 같이 있지 못했지만 그래도 차분한 말투로 여러가지를 가르쳐 주셨던 지웅이형, 문수형 그리고 저의 사수이셨던 재혁이형에게 감사의 말씀을 전합니다. 익숙지 않은 대학원이라는 환경에 멤버들과 빠른 시간 내에 편해질 수 있었던 건 아마 형 덕분이 아닐까 생각합니다. 형광체에 관하여 아무것도 모르는 저를 형광체 팀으로 받아주고 1 년 반 동안 같이 연구하며 많은 조언과 아이디어를 제시해준 형께 감사 드립니다. 늘 웃음과 재미를 추구해준 재희형! 형의 조언들이 없었으면 정말 힘들었을지 몰라요. 지난 1 년동안 같이 운동하면서 이런 저런 예기들로 많이 배우고 즐겁게 생활한 것 같습니다. 앞으로도 부탁드리고 감사합니다. 그리고 우리 잘라인 홍횽!ㅋ (말좀…해주세요… 늘 조용히 말없이 도와주심에 감사드립니다. 다시 잘라인 탑으로 올라오셔야죠;) 그리고 재철형님! 형광체 팀에 들어와서 형과 함께 커피마시면서 들은 실험적, 또한 그 외적 조언들 너무나도 감사드립니다. 앞으로도 저희 형광체 팀을 잘 이끌어주세요!!ㅎ 우리 또 한명의 운동멤버 충권이형! 형하고도 운동하면서 많은 조언과 많은 지지해주신점 감사드립니다. 이제는

써멧장이신데 꾸준히 좋은 결과 나오길 바랄게요. 다음학기에도 운동 같이해요~ 나랑 동갑인 6 개월 먼저 들어온 지선이! 가끔 너의 말도 안되는 개그는 아직도 어색하지만 그래도 너의 그 개그코드덕분에 실험실에 웃음이 많은거 같아. 이젠 좀 자제해줘.ㅋ 그리고 멋있는 노숙자 현재형! 앵그리 상우와 히드라 대권이 6 개월 정도밖에 아직 같이 지내진 않았지만 정말 멋진 후배가 들어와서 기분이 좋구나. 앞으로도 같이 열심히 실험하고 좋은 결과 만들어보자! 마지막으로 외국인 친구들. 마흐디! 한국에 와서 힘들텐데 잘 지내는거 보면 참 멋지네요. 한국에서 더 좋은 추억 만들고 가세요! 실험도 열심히 베이스도 열심히 하시는 빠뚜형! 앞으로 남은 6 개월동안 파이팅 하시고 좋은 결과로 졸업하길 기도할께요! 우리 CMC 사람들께 더 많은 글을 적고싶지만 전 떠나느게 아니니 여기서 이만 줄이겠습니다. 감사합니다.

또한, 제 인생에서 소중한 가족과 친구들께 감사의 글을 적습니다. 저를 이 자리에 있게 해주신, 부족하지만 언제나 제가 하고싶은 일을 실천할수 있게 아낌없이 지원해주신 부모님께 감사의 말씀을 전해드리고싶습니다. 그리고 언제나 따뜻하게 감싸주고 힘이 되어준 누나에게도 감사의 말씀을 전합니다. 바쁘다는 핑계로 연락도 잘 하지 못했는데 앞으로는 좀 더 나은 아들이 되도록 노력하겠습니다. 또한 가끔씩 저에게 재미를 던져주는 멋쟁이 빈이삼춘! 감사합니다.

영국에서부터 지금까지도 인연이 닿아 한국에서도 좋은 추억을 쌓은 IC 멤버들. 태성아! 너도 이제 몇 개월 안남았는데 파이팅 하자! 이제 갖 군대에 입대한 정훈이, 군생활중인 우명이, 군생활 열심히 하고 건강하게 2 년 보내다 와라! 기다린다! 내 뒤를 늘

쫓아오는 동준아! ACS NANO 진심으로 축하한다! 남은 6 개월 열심히 하고 졸업 잘해! 너 졸업하고 떠나면 커피는 누구랑 마시니… 이제는 애 아빠가 된 정준이… 힘들때 늘 힘을 실어줬었는데, 미국에서 공부 맞추고 대박내서 한국에 오렴. 공군 장교 한두! 너도 이제 몇 개월 안 남았구나! 말년 잘 보내고 서울에서 자주 보자! 서울대에 들어오면서 후배가 선배로 바껴 버린 민이누나, LG 에서도 열심히 해! 아직 영국에 있지만 종종 연락하는 내 과 동기인 택보랑 수나누나. 박사졸업 미리 축하할게! 이름은 다 넣지 못했지만 영국 멤버들, 친구들, 말로 표현하기 부족하지만 고맙다는 말씀을 전하고 싶습니다.

2013 년 07 월 31 일, 이문균